Spatially continuous snow depth mapping by airplane photogrammetry for annual peak of winter from 2017 to 2021 in open areas

Leon J. Bührle[1,2], Mauro Marty[3], Lucie A. Eberhard[1,2,4], Andreas Stoffel[1,2], Elisabeth D. Hafner[1,2,5], Yves Bühler[1,2]

[1] WSL Institute for Snow and Avalanche Research SLF, Davos Dorf, 7260, Switzerland
[2] Climate Change, Extremes and Natural Hazards in Alpine Regions Research Center CERC, 7260 Davos Dorf, Switzerland
[3] Swiss Federal Institute for Forest, Snow and Landscape Research WSL, Birmensdorf, 8903, Switzerland
[4] Institute of Geodesy and Photogrammetry, ETH Zurich, Zurich, 8092, Switzerland
[5] EcoVision Lab, Photogrammetry and Remote Sensing, ETH Zurich, Zurich, 8092, Switzerland

Correspondence to: Yves Bühler (buehler@slf.ch)

Abstract.

Information on snow depth and its spatial distribution is important for numerous applications such as the assessment of natural hazards, the determination of the available snow water equivalent ~~(SWE)~~ for hydropower, the dispersion and evolution of flora and fauna and the validation of snow-hydrological models. Due to the heterogeneity and complexity of snow depth distribution in alpine terrain, only specific remote sensing tools are able to accurately map the present variability. To cover large areas (>100 km²), airborne laser scanners (ALS) or survey cameras mounted on piloted aircrafts are needed. Applying the active ALS leads to considerably higher costs compared to photogrammetry but also works better in forested terrain. The passive photogrammetric method is more economic but limited due to its dependency on good acquisition conditions (weather, sufficient light~~, contrast on the snow surface~~). In this study, we demonstrate the reliable and accurate photogrammetric processing of high spatial resolution (0.5 m) annual snow depth maps during peak of winter over a 5-year period under different acquisition conditions within a study area around Davos, Switzerland. Compared to previously carried out studies, using the new Vexcel Ultracam Eagle M3 survey sensor~~,~~ improves the average ground sampling distance ~~(GSD)~~ to 0.1 m at similar flight altitudes above ground. This allows for very detailed snow depth maps ~~of~~in open areas, calculated by subtracting a snow-free digital terrain model (DTM acquired with ALS) from the snow-on digital surface models (DSMs) processed from the airborne imagery. Despite complex acquisition conditions during the recording of the Ultracam images (clouds, shaded areas and new-snow cover), 99 % of unforested areas were successfully reconstructed. We applied masks (high vegetation, settlements, water~~s~~, glaciers) to significantly increase the reliability of the snow depths measurements. An extensive accuracy assessment including the use of check points, the comparison to DSMs derived from unpiloted aerial systems ~~(UAS)~~, and the comparison of snow-free pixels to the ALS-DTM prove the high quality and accuracy of the generated snow dept~~hs~~ h maps. We achieve a root mean square error ~~(RMSE)~~ of approximately 0.25 m for the Ultracam X and 0.15 m for the successor sensor

Ultracam Eagle M3. By developing an almost ~~automated,~~ consistent and reliable photogrammetric workflow for accurate snow depth distribution mapping over large regions, we provide a new tool for analysing snow distribution in complex terrain. This enables more detailed investigations on seasonal snow dynamics, can be used for numerous applications related to snow depth distribution as well as avalanches and serves as ground reference for new modelling approaches as well as satellite-based snow depth mapping.

1 Introduction

Accurate snow depth mapping is important for the assessment, prediction and prevention of natural hazards such as snow avalanches or floods. Crack propagation and the size of release areas of snow avalanches are, f~~F~~or example, linked to snow depth distribution (Veitinger und Sovilla 2016; Schweizer et al. 2003). ~~crack propagation and the size of release areas of snow avalanches are(Veitinger und Sovilla 2016; Schweizer et al. 2003)[56]. The release volume and the length of avalanche runouts particularly depend on the releasing and eroded snow volumes.~~ The snow distribution, and therefore avalanches, are simultaneously influenced by wind induced s~~S~~now-drift ~~caused by wind and its influence on the snow distribution~~ in the starting zone a~~nd~~s~~w~~ well as the avalanche path ~~is another key parameter for avalanches~~(Schön et al. 2015). Further hazards related to snow depth~~s~~ are snow loads on buildings, threatening not only the stability of roofs but potentially leading to dangerous roof avalanches ~~snow slides from roof~~(Croce et al. 2018)(Croce et al. 2018). Additionally, snow depth and the corresponding snow water equivalent (SWE) ~~of the snowpack~~ are crucial for flood~~the forecast of floods~~forecasting~~the forecast of floods during snowmelt periods~~. Various economic sectors can benefit from accurate snow depth information~~.~~, f~~ F~~or example, the available SWE ~~within catchments~~ is a key criterion for the implementation and operation of hydropower (Magnusson et al. 2020). Detailed information on snow depth distribution on slopes is also valuable for ~~the decision-makers of~~ winter resorts(Spandre et al. 2017). Moreover, snow depth mapping facilitates research on interactions between snow depth distribution and flora as well as fauna ~~/~~(Wipf et al. 2009)., ~~because snow depth distribution determines the growth of plants and shapes the habitats of mountain animals.~~

Precise snow depth measurements are key data when ~~developing and~~ validating models for snow parameters. ~~For~~In avalanche modelling tools such as the Rapid Mass Movement Simulation (RAMMS) (Christen et al. 2010) ~~or SAMOS-AT (Sampl und Zwinger 2004)~~, the snow volume derived from snow depth maps ~~in the starting zone andas well as in the deposition zone~~ can be compared to modelled results. Furthermore, snow depth maps~~they~~ can serve as reference ~~datasets~~ for snow depth distribution models (Wulf et al. 2020) and snow-hydrological models like Alpine3D (Richter et al. 2021; Schlögl et al. 2018; Vögeli et al. 2016; Brauchli et al. 2017), Factorial snowpack model (FSM) (Essery 2015) and Crocus (Brun et al. 1992). ~~Snow depth maps can also improve crucial input data for snow hydrological models likesuch as precipitation by serving as a precipitation scaling parameter (Vögeli et al. 2016; Brauchli et al. 2017).~~ From high spatial resolution snow depth maps, the

fractional snow-covered area parameter~~,~~ can be also compiled ~~the derivation of the standard deviation of snow depths during peak of winter is feasible, and can be used for various model applications~~ (Helbig et al. 2021).

Traditionally, snow depth is measured by field observations such as manual probing or by automated weather stations (AWS). However, ~~to get spatially continuous coverage, interpolation is required~~ interpolation is required to get a spatially continuous coverage. As snow depths vary a lot over short distances, especially in complex terrain (Grünewald et al. 2010; Grünewald et al. 2014), interpolation is insufficient for most applications~~ and has been shown to result in very large errors~~. Ground-penetrating radar (GPR) can capture many point measurements when mounted on a sledge or snowmobile (Helfricht et al. 2014) with a high accuracy of less than 0.1 m (Griessinger et al. 2018). Still, only transects and ~~not~~ spatially non-continuous snow depth distribution are measured (McGrath et al. 2019). ~~In addition, very steep and poorly accessible terrain cannot be covered and the method is only practicable for small catchments, if no helicopter is available .~~

Remote sensing tools can provide accurate and spatially continuous snow depth measurements. Terrestrial laser scanning (TLS), based on the reflectance of laser beams on object surfaces, can provide very exact measurements (Deems et al. 2013). The achieved accuracy depends on the sensor and the object's distance from the scanner and ranges~~is ranging~~ from 0.05 m to 0.2 m in distances below 1000 m (Grünewald et al. 2010; Prokop 2008) and 0.3 m to 0.6 m over longer distances of around 3000 m (López-Moreno et al. 2017). ~~Other crucial advantages are a lower weather dependency regarding the illumination conditions~~ Another crucial advantage~~s~~ is the lower weather-dependency regarding the illumination conditions~~ and possible measurements in vegetated areas, if suitable scanner locations with a sufficient measurement angle are available~~. Limitations of this procedure are the access to locations for the scanner and the occurrence of concealed areas which cannot be measured as well as poor weather conditions such as strong snowfall ~~or fog~~ (Prokop 2008).

In recent years, the use~~importance~~ of digital photogrammetric methods has increased mainly due to the development of the SIFT-algorithm (Lowe 2004), easy to apply software~~s~~ like Agisoft Metashape or Pix4D and the development of unpiloted aerial systems (UAS). ~~Various publications have confirmed the high accuracy of snow depths derived from UAS photogrammetry.~~ The accuracy ~~of snow~~of snow depths derived from UAS photogrammetry, which mainly depends on the sensor, the ground sampling distances (GSD) as well as collection conditions,~~ –~~ ranging from~~of~~ 0.05 m to 0.2 m (Bühler et al. 2016; Michele et al. 2016; Harder et al. 2016). Critical issues for this method are the dependency on good weather and light conditions (Bühler et al. 2017; Gindraux et al. 2017) and the difficulties of measuring snow depths in areas with high vegetation. Unpiloted aerial laser scanning systems (ULS) combine the advantages of TLS and UAS and can measure snow depths with a high accuracy of around 0.1 m in unforested (Jacobs et al. 2021) and~~as well as~~ 0.2 m in forested terrain (Harder et al. 2020). However, the current UAS, ULS and TLS can only capture areas up to 5 km² (Revuelto et al. 2021).

To map larger regions, airborne laser scanners (ALS), airplane photogrammetry ~~optical cameras mounted on piloted airplanes~~ or satellites are needed. ~~The increased spatial resolution of imagery from optical satellites such as~~For satellites, both Pléiades and Worldview-3, offer~~combined with their~~ high temporal resolution and trough (triple) stereo ~~acquistions~~acquisitions ~~and availability of near-infrared (NIR) bands enable~~allow for ~~new possibilities for~~ large-scale snow depth mapping (Marti et al. 2016). However, ~~F~~first studies have ~~however~~ shown that snow depth measurements from Pléiades imagery in comparison to reference data exhibit a ~~deviations~~ root mean square error (RMSE) of more than 0.5 m (Deschamps-Berger et al. 2020; Eberhard et al. 2021; Shaw et al. 2020). ~~. For example, Marti et al. (2016) calculated a normalized median absolute deviation (NMAD) value of 0.78 m compared to snow depth measurements derived from UAS. Other studies researching the application of Pléiades achieved a root mean square error (RMSE) relative to reference data of 0.5 m (Eberhard et al. 2021; Shaw et al. 2020) to 0.8 m (Deschamps-Berger et al. 2020).~~ These accuracies do not satisfy the requirements for most snow depth mapping applications. The study of McGrath et al. (2019) applied the WorldView-3 satellite with a GSD~~spatial resolution~~ of 0.3 m (resampled to 8 m grid) ~~–~~and achieved a considerably higher accuracy with a RMSE of 0.24 m compared to GPR. ~~The dependency of optical satellite sensors on cloud-free conditions stimulates the application of active satellite sensors with synthetic aperture radar (SAR), which are independent from light and weather conditions (Tsai et al. 2019). However, their spatial resolution is currently not sufficient for detailed and accurate snow depth measurements (Lievens et al. 2019; Lievens et al. 2022).~~

In contrast to satellite measurements, ALS ~~fulfils the criteria for accurate snow depth mapping over large areas. Different studies have proven, that the~~ achieves accuracy~~y~~ies~~, which depends on the flight altitude ,~~ ~~is~~ similar to the one of TLS (Mazzotti et al. 2019; Deems et al. 2013). However, Bühler et al. (2015) estimated the cost for an ALS-flight and the processing of the data to be around 50’000 to 80’000 CHF~~CHF~~, covering an area of 150 km². Current inquiries on different companies confirm ~~T~~these high costs, which ~~–~~prevent the realisation for many implementations. Airplane-based photogrammetry, however, is more economic with costs ranging from 30’000 to 60’000 ~~$~~CHF for the same area~~CHF~~ (Bühler et al. 2015). Despite the application of a lower cost camera (Nikon D800E), Nolan et al. (2015) successfully created snow depth maps over small areas (5 - 40 km²) and reached an excellent accuracy of about 0.1 to 0.2 m. Bühler et al. (2015) ~~also~~ produced a high-resolution snow depth map with a spatial resolution of 2 m, covering a heterogeneous high-mountain area of 300 km² around Davos. Using the surveying pushbroom-scanner Leica ADS 80, a RMSE of 0.3 m comparing to GPR, TLS and ~~manual~~ probing was achieved. ~~-~~Meyer et al. (2022) created ~~one~~ a snow depth map~~s~~ with ~~a~~ 1 m spatial resolution covering an area of 300 km² ~~-~~and demonstrated that airplane-based photogrammetry can reach accuracies similar to the ones of the ALS. The new state ~~-~~of ~~-~~the art 450 Megapixel ~~(MP)~~(MP) frame sensor Vexcel Ultracam Eagle M3 can record extremely high spatial resolution images, which enables the generation of accurate large-scale digital surface models (DSM). ~~accurate digital surface models (DSM) of large regions.~~ Eberhard et al. (2021) achieved an accuracy of around 0.1 m using the Vexcel Ultracam Eagle M3 as well as 29 ground control points (GCPs) to refine the orientation within a small catchment (4~~3~~0 km²).

In this study, we present the consistent processing of five annual snow depth maps with a spatial resolution of 0.5 m based on Vexcel Ultracam images covering approximately 2350 km² each year. These datasets were acquired at peak of winter, ~~which was characterized by~~capturing large differences in ~~snow cover and~~ average snow depths as well as~~,~~ ~~under~~ various weather and illumination conditions were observed between the different years~~. Complementing the existing snow depth maps from 2010 to 2016 (2 m spatial resolution) (Bühler et al. 2015; Marty et al. 2019) these unique data series enables the long-term monitoring of snow depth distribution in high alpine terrain~~.

2 Study area Davos, Switzerland

The study area is located around Davos in eastern Switzerland. A core area with an extent of approximately 2340 km² was covered by all flight campaigns from 2019 to 2021. However, the total area acquired per year differs due to ~~V~~varying flight routes during image recording ~~acquisition~~ (Figure 1)~~ resulted in different extents of the derived snow depth maps~~. ~~However, the core area with an extent of 240 km² was covered by all flight campaigns from 2019 to 2021 and will also serve as the study area for the prospective snow depth maps. Various regions of the research area, for example, the Weissfluhjoch (Wirz et al. 2011), the Wannengrat (Schirmer und Lehning 2011), the Dischma Valley (Grünewald et al. 2014; Bühler et al. 2015; Eberhard et al. 2021), and the Flüela Valley (Bühler et al. 2016) were already part of snow depth mapping studies (Fig. 1).~~

The elevation of the main study area ranges from 1100 m a.s.l around Klosters to the 3229 m a.s.l. high Piz Vadret. The diversity of the terrain, including extremely steep faces, large heterogeneous as well as open areas, settlements, ~~heavily~~ forested and glaciated areas ~~as well as extremely steep faces,~~ is representative for many mountain regions. ~~The elevation of the main study area is ranging from~~ranges from ~~1100 m a.s.l around Klosters to the 3229 m a.s.l. high Piz Vadret.~~ The research area is located in a transition zone between the humid north-alpine climate and the drier climate zone of the central A~~a~~lps~~, which is significantly drier~~ (Kulakowski et al. 2011; Mietkiewicz et al. 2017). The main snowfall in the winter season is recorded during north-westerly and northern weather situations, which are commonly connected to strong storms with high wind speeds (Gerber et al. 2019; Mott et al. 2010). ~~The date of the peak of winter in this region is usually between March and April at an elevation of approximately 2000 m a.s.l..Previous investigations have shown, that the average snow depth of the study area varies a lot~~

~~135 and can range from around 1 m to 2.5 m (Marty et al., 2019).~~

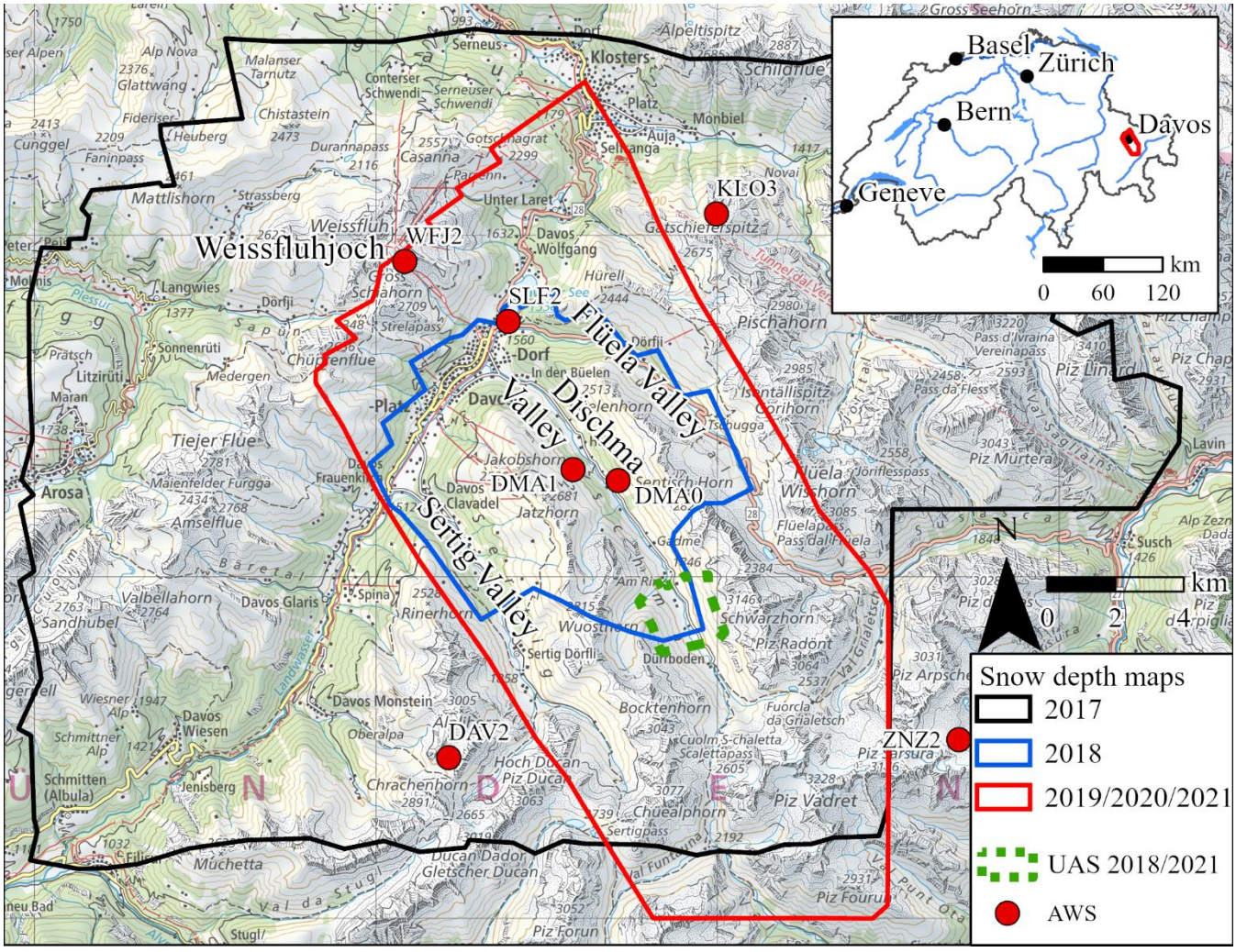

Figure 1. Overview of the study area: Snow depth map generated by the airplane 2017 (black), extent of snow depth map from 2018 (blue) and snow depth area derived from the respective flights in 2019, 2020 and 2021 (red; corresponds to main study area). Additionally, the area covered by the UAS for reference data in 2018 and 2021 are shown (green). The red points symbolise~~ic~~ the location of the automatic weather stations with accurate snow depth measurements. The red polygon in the inset map depicts the location of the main study area in Switzerland (map source: Federal Office of Topography).

3 Data and sensor

3.1 Vexcel Ultracam

Airborne imagery was acquired with the survey camera Vexcel Ultracam series. The Vexcel Ultracam X was applied in 2017, and is characteri~~s~~z~~z~~ed by a sensor pixel size of 7.2 µm x 7.2 µm, a focal length of 100.5 mm and a resolution of 14430 x 9420 ~~x 14430~~ pixels (Schneider und Gruber 2008). Due to better characteristics of the ~~successor~~ camera Ultracam Eagle M3, the Ultracam X was replaced in the following years. The Ultracam Eagle M3 belongs to the current state-of-the art cameras for

photogrammetric measurements with 450 MP (Bühler et al. 2021). The improvements include a ~~better~~ sensor pixel size of 4 µm x 4 µm, a focal length of 120.7 mm and a ~~better~~ resolution of 26000 x 14000 pixels (Eberhard et al. 2021). Both Ultracam cameras ~~simultaneously~~ acquire the four spectral bands red-green-blue (RGB) and NIR with a radiometric resolution of 14 bits. The camera positions are registered by differential global navigation satellite system (DGNSS) mounted at the camera with a nominal accuracy of 0.2 m. The orientation of the camera is recorded through an inertial measurement unit (IMU) with a nominal accuracy of 0.01° (omega, phi, kappa). This data simplifies the determination of interior orientation and the correct georeferencing and prevents tilts of the DSM.

The flights were conducted during the expected peak of winter (at approximately 2000 m) between March and April around midday to avoid large, shaded areas. The exact extent of each flight varied from year to year and is based on the ~~authorized~~ flight route and~~,~~ weather conditions ~~and occurrence of technical problems~~ (Fig. 1). The captured region in 2017 covered 600 km² (Fig. 1, black polygon) and was considerably larger than in the following years. High costs and limited flight permissions resulted in the selection of a smaller main study area (250 km², red polygon) around Davos for the subsequent years.

~~Simultaneously to~~Before the flights, reference points were marked with specially patterned ~~musterned~~ tarps and measured by DGNSS with a vertical accuracy of 0.05 m. Because no reference points were acquired in 2017 and 2019, ten extra reference points on conspicuous road markings were measured in retrospect. Different characteristics ~~and special features~~ of each flight are described in ~~the~~ Table 1.

Table 1. Properties of the executed annual Ultracam flights during peak of winter.

Acquisition date	Sensor type	Reference points	Mean GSD [m]	Mean flight altitude [m above ground]	Notice
16 March 2017	Ultracam X	0	0.23	3430	Large, shaded areas, inaccuracies of NIR-band
11 April 2018	Ultracam Eagle M3	8	0.06	1780	Technical problems (airplane), heavily cloudy
16 March 2019	Ultracam Eagle M3	0	0.12	4040	Only RGB-bands, no NIR-band
6 April 2020	Ultracam Eagle M3	38	0.12	3970	Good conditions
16 April 2021	Ultracam Eagle M3	14	0.12	3910	few clouds in the east and west part, new snow

3.2 Reference dataset

3.2.1 Airborne laser scanner (ALS) from summer 2020

Calculating snow depths with photogrammetric methods requires an accurate snow-free reference dataset. For the ~~main part of the~~ study area, an ALS point cloud ~~-~~from summer 2020 was available (Federal Office of Topography swisstopo 2021a). The specified accuracies of at least 0.2 m in horizontal and 0.1 m in vertical direction comply with the requirements of accurate snow depth mapping. The point density of the ALS point cloud of at least 10~~5~~ points m^{-2} and on average 20 points m^{-2} for all returns as well as 15 points m^{-2} for ground returns allows a rasterization of 0.5 m and the exact reconstruction of small-scale features as well as~~nd extremely~~ steep faces. The exact point classification enables the separation of vegetation, ground, buildings and water~~s~~ bodies. Correspondingly, a digital terrain model (DTM), a normalized ALS-DSM which only considered vegetation and a normalized-DSM which only took buildings into account were processed from the ALS point cloud. ~~Due to the high point density, a rasterization to a spatial resolution of 0.5 m was performed~~applied. The ALS-DTM also served as a reference dataset to evaluate the accuracy of the snow depth maps through the comparison of snow-free areas.

3.2.2 Unpiloted aerial systems (UAS) photogrammetry 2018 and 2021

To ~~compare~~analyse spatial snow depths of small catchments, UAS-derived DSMs are commonly used, given the flexible acquisition at a vertical accuracy of often better than 0.1 m (Bühler et al. 2016). ~~Therefore~~In order to compare snow depths derived from airborne data to UAS derived ones, two UAS flights were carried out for a small subset (3.5 km²) in the Dischma

Valley during the Ultracam flight campaigns in 2018 and 2021 (Fig. 1, green polygon). ~~Short-term technical problems on the airplane in~~In 2018 ~~prevented the simultaneous capture of the~~ there was a small-time lag (4 days) between UAS (eBee+ RTK) and airborne data acquisition. No significant snowfall, but slightly positive temperatures (0°C level at 2500 m) were registered in between ~~the recording of the UAS and the airborne data.~~ In 2021, the UAS acquisition was conducted simultaneously to the Ultracam flight by the ~~vertical take-off and landing (VTOL) drone~~ WingtraOne drone with a 42 MP camera. The processing workflow of the UAS-derived DSMs was similar to the ~~described~~ approach described in Eberhard et al. (2021) with the ~~crucial~~ only difference that outliers of the point cloud (less than 3 depth maps) ~~were identified and excluded~~were excluded. ~~Outliers were removed by the confidence interval of less than 3 depth maps. The achieved accuracy of the DSMs was identified by using check points (CP) with a RMSE of 0.06 m (2021) and 0.1 m (2018).~~

3.2.3 Manual reference points

The manually measured reference points during the Ultracam flights had the purpose of serving as GCPs or check points (CPs). Due to the time-consuming ~~and expensive~~ fieldwork as well as the ~~presenting~~ avalanche danger, the number of reference points was limited, and they were often located close to ~~streets~~roads in flat terrain. The ten points measured in retrospect at distinctive ~~and unambiguous~~ locations were valid as reference, although they have a lower reliability compared to directly measured reference ~~points.~~

~~Only~~points. ~~Only i~~In 2020, during low-level avalanche danger, 40 reference points could be placed well distributed ~~over~~ at different elevations and ~~on various~~ aspects.~~.~~

4 Methods

The creation of reliable and accurate snow depth maps consists of four steps (Fig. 2):

- Processing of airborne imagery and ALS point cloud
- Calculation of snow depths
- Creation and application of necessary masks
- Accuracy check of the finalized snow depth maps

~~Using the same coordinate system for all processing steps is fundamental to prevent offsets.~~ The horizontal coordinate system CH1903+ LV95 and the height reference system LN02 were ~~selected due to their common application in Switzerland~~used for the processing of data. To ensure that the same coordinate system was used for all input data, ~~C~~conversions from other coordinate systems were carried out with the tool REFRAME (Federal Office of Topography swisstopo 2021b)~~[sic]~~ and transformations available in ArcGIS Pro 2.7. The processing of airborne imagery was realized in Agisoft Metashape 1.6~~, an easy-to-use software for photogrammetric applications~~. It~~Agisoft Metashape~~ has proven its value in numerous snow-related studies (Avanzi et al. 2018; Bühler et al. 2016) and allows the processing of very large high spatial resolution airborne images (Eberhard et al. 2021; Meyer et al. 2022). The calculations and modifications of the snow depth values were realized in ArcGis Pro. ~~Handling numerous very high resolution images requires a high-end hardware setup. We used an Intel® Xeon Platinum 8267 2.9 GHz processor (48 cores), 383 GB of memory and six NIVIDIA GeForce RTX 2080 TI`s with 12 GB of graphic memory. The processing time of each Ultracam dataset was approximately two days.~~

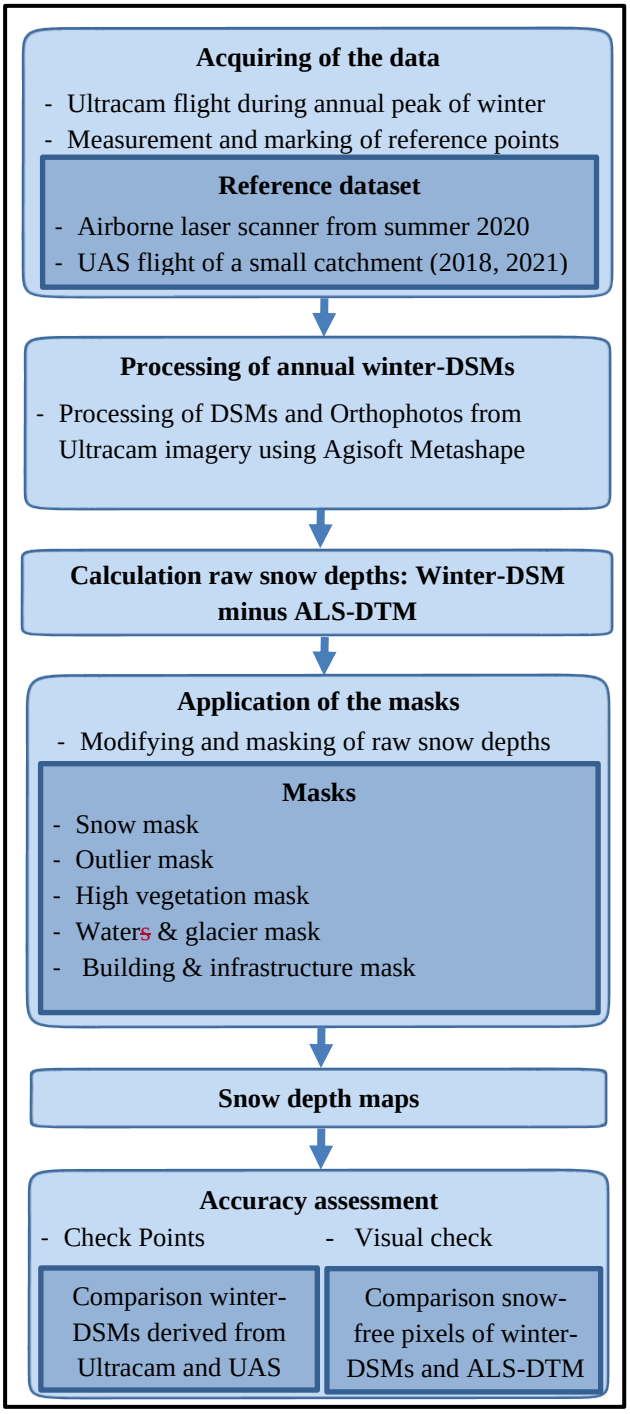

Figure 2. Flowchart illustrating all processing steps for the creation of snow depth maps.

4.1 Processing workflow of airborne imagery

The processing of aerial images in Agisoft Metashape is based on the Structure from Motion ~~(SFM)~~ algorithm (Koenderink und van Doorn 1991; Westoby et al. 2012). The general workflow is well-explained in various publications (Adams et al. 2018) and in the Agisoft manual (Agisoft LLC 2020). However, the existing framework conditions of this study, applying the ~~-~~new ~~high resolution~~ sensor Vexcel Ultracam in combination with such a large and heterogeneous study area are sparsely explored.

~~-~~Only Eberhard et al. (2021) successfully generated a winter-DSM derived from Ultracam imagery. Therefore, the workflow used in this study is based on Eberhard et al. (2021). However, the aim to use as few as possible GCPs to refine the orientation due to the limited availability of reference points required an adaption of this workflow.

The Vexcel Ultracam camera is ~~regularly~~ calibrated, hence the interior orientation is known exactly. However, the application of the calibrated lens distortion parameters led to a large offset of the z-value in the resulting DSM of approximately 2 m. Therefore, the interior and exterior orientation were calculated in Agisoft Metashape during the bundle-adjustment process (Triggs et al. 2000). Subsequently, the parameters for the interior and exterior orientations (especially focal length) were improved by the application of two to five GCPs. The necessary number of GCPs and the influence of their distribution for an exact and reliable orientation was determined by a parameter study for the Ultracam flight in 2020, which was characterized by 40 well-distributed reference points (Table A1). The quality grade was ascertained by the calculated RMSE of the check points, which were not used for the orientation of the model (Agisoft LLC 2020). This approach has shown that ~~the use of~~ only one GCP is sufficient for a correct orientation and determination of atmospheric distortions under favourable acquisition conditions. ~~Warps and tilts, which often occur using a low number of GCPs with a limited dispersion over the area, were avoided because of the availability of the exact coordinates of the shutter release~~

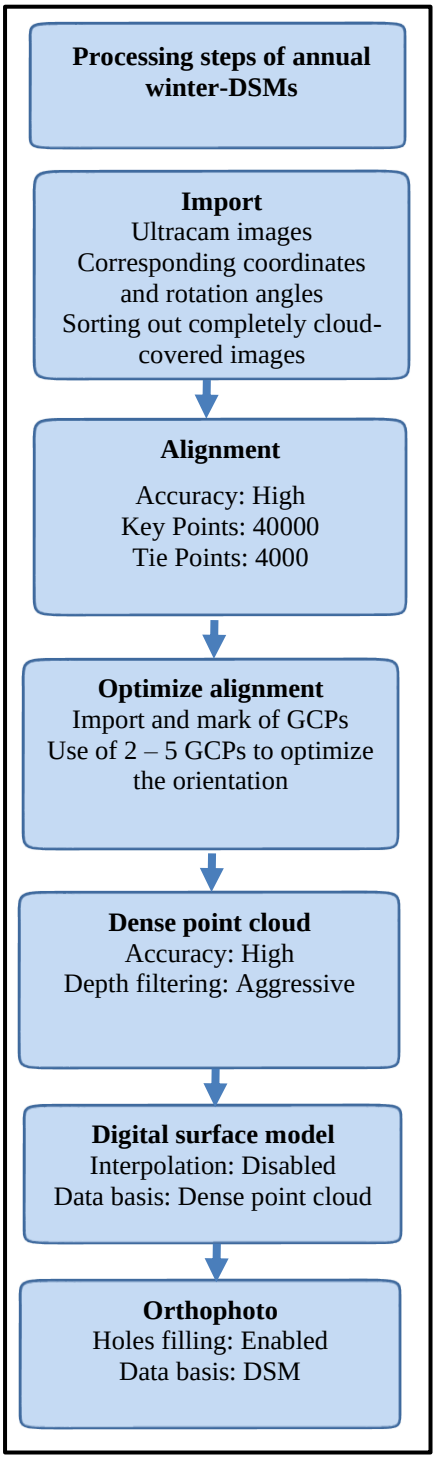

Figure 3. Flowchart illustrating the workflow generating the winter-DSMs on the basis of Ultracam images.

~~points and the rotation angles of the camera.~~ Using more and well distributed GCPs had no significant influence on the quality grade (Table 2). However, due to the high dependence on the precise measurement when using only one GCP, and the possibility of varying atmospheric distortions when using cloud-covered images, ~~the~~we recommend the ~~implementation~~use of two to five GCPs ~~is to be preferred~~. Warps and tilts, which often occur using a low number of GCPs with a limited dispersion over the area, were avoided because of the availability of the exact coordinates of the shutter release points and the rotation angles of the camera.

Table 2. Overview of the settings used and the corresponding accuracy (RMSE) for the parameter study for 2020.

Pre-calibration	Used dGNSS coordinates	Used rotation angles	Number and distribution GCPs	RMSE (Z; Total) [m]
✓	✓	✓	-	2.19; 2.20
✘	✓	✓	-	1.04; 1.08
✘	✓	✓	15	0.07; 0.15
✘	✓	✓	4 (Davos, Dischma~~Dischma~~, Sertig)	0.07; 0.155
✘	✓	✓	3 (Davos, Dischma, Frauenkirch)	0.08; 0.16
✘	✓	✓	1 (Davos)	0.08; 0.17

The final DSMs with a point density from 5 points m^{-2} (2017) over 20 points m^{-2} (2019 – 2021) up to 90 points m^{-2} ~~/m²~~ (2018) and the corresponding orthophotos were exported with a spatial resolution ranging from 0.1 to 0.45 m~~m~~ , ~~-~~depending on the average GSD. The workflow used is illustrated in Fig. 3 and further settings are described in Eberhard et al. (2021).

4.2 Creation of snow depth maps

The snow depths were calculated by subtracting the photogrammetric winter-DSM from the ALS-DTM resulting in~~. The improved spatial resolution of the Ultracam based DSMs and the ALS DTM (0.5 m) enables the creation of~~ snow depth maps with a spatial resolution of 0.5 m~~. Therefore, the~~ using the resampled winter-DSMs ~~were resampled to a resolution of 0.5 m~~. To avoid uncertainties based on misalignments between the winter-DSM and the ALS-DTM, we checked deviations of snow-free pixels in steep areas in each snow depth map. ~~Due to~~ Since the deviations were small and the number of snow-free pixels in some years were limited, we did not perform a co-registration. The use of an ALS-DTM was preferred ~~Ddue to~~because a DSM would underestimate the snow depths in open areas with low vegetation (Eberhard et al. 2021; Feistl et al. 2014)~~low~~

~~vegetation is often compressed by snow in winter~~ (Feistl et al. 2014)~~,~~ ~~the application of an ALS-DTM was preferred over an~~ ~~ALS-DSM, as the use of a DSM would underestimate the snow depths in regions with low vegetation~~ (Eberhard et al. 2021)~~.~~ In addition, photogrammetric methods often struggle in ~~the~~ dense and steep forests as well as in settlements in our study area, where the ALS-DSM would have crucial advantages (Bühler et al. 2015)~~.~~ ~~Nevertheless,~~ To get accurate and reliable snow depth maps, the application of various masks was required. Without the application of these masks, the average snow depth value of the study area would be overestimated by approximately 1 m, mainly caused by the forested areas.

~~using a DTM leads to extremely high and unrealistic snow depths in settlements and forested areas, which both have a high influence on various statistics of the snow depths. Consequently, these areas exhibit many inaccuracies of photogrammetric measurements and they are not suitable for accurate snow depth mapping. Furthermore, different characterizations of high vegetation regarding its behaviour in the winter months complicates the assessment of the actual snow depth~~ (Eberhard et al. 2021)~~.~~

~~To get accurate and reliable snow depth maps, the application of various masks was~~ The~~is~~ procedure for developing these masks is based on the approach of Bühler et al. (2015), improved by Bührle (2021) and contains a snow, an outlier, a high vegetation , a water~~s~~ and glacier mask as well as an infrastructure and building mask. However, the existing algorithm to calculate the masks was adapted due to the use of the better Ultracam sensor and the availability of an accurate and well-classified ALS point cloud. ~~Without the application of these masks, the average snow depth value of the study area would be overestimated by approximately 1 m.~~ An important ~~other~~ goal for the procedure is the consistent and reproducible ~~automatic~~ creation of the masks~~. Correct snow depth maps depend on the implementation of the masks in the workflow presented~~ (Fig. 4). Additionally, e~~E~~xcluding regions with heavy cloud-cover and outlying areas led to more reliable snow depth values.

4.2.1 Snow Mask

The snow mask has the aim to modify calculated snow depths of snow-free areas to zero (Bühler et al. 2016). Therefore, each pixel of the corresponding orthophoto is classified ~~into~~ as ~~the categories~~ snow-covered or snow-free, using the Normalized D~~d~~ifference S~~s~~now I~~i~~ndex (NDSI)~~ classification~~ (Dozier 1989; Hall et al. 1995) with a threshold around 0. This approach was applied for the years 2017, 2020 and 2021. ~~Technical issues in 2019 prevented the recording of the NIR-band and accordingly to this no NDSI classification could be processed.~~ A NDSI classification was not done in 2019 due to technical issues that prevented the recording of the NIR-band.~~In 2018, the NDSI classification falsely classified many artefacts such as snow mixed with soil as snow free~~ In 2018, the NDSI method falsely classified pixels that exhibited snow mixed with soil as snow

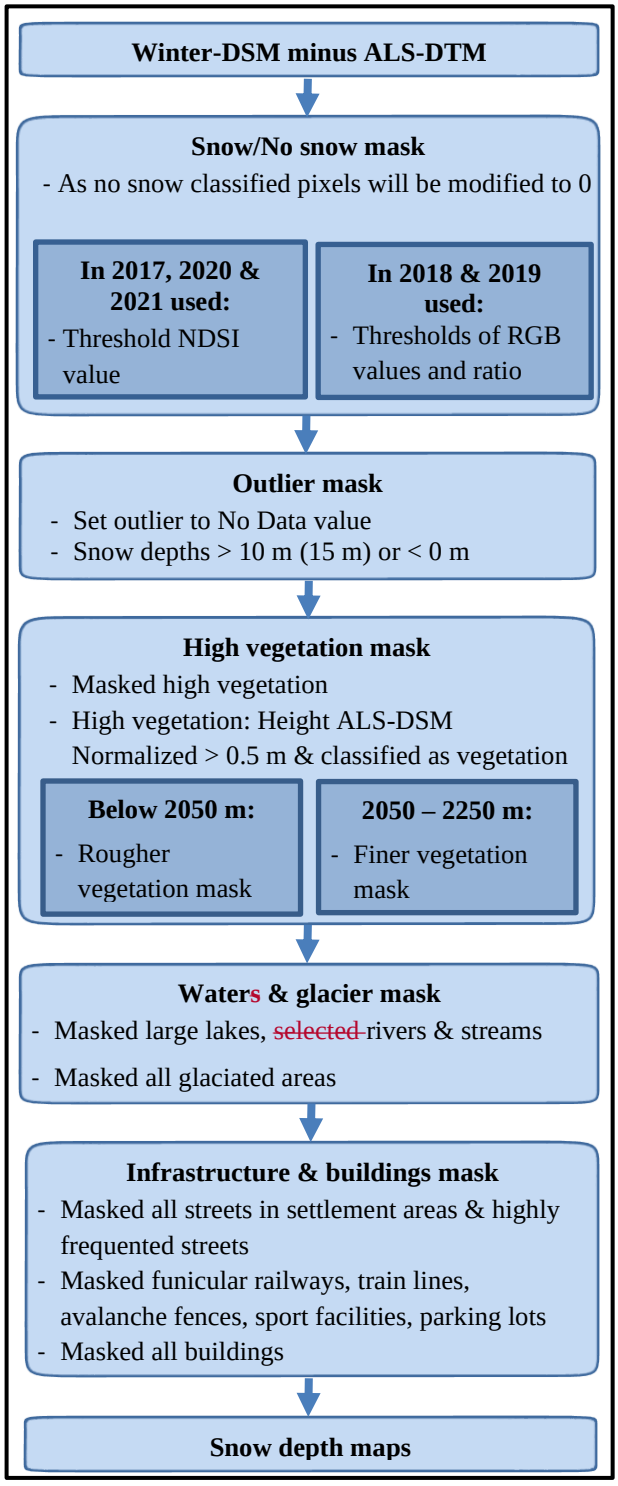

Figure 4. Flowchart illustrating the various masks used for the generation of reliable snow depth maps.

free. Therefore, another classification method without the necessity of the NIR-band and a better operation in snow mixed with soil, was required. Since the blue band of snow exhibits higher reflectance than the red and green band (Eker et al. 2019) a threshold of the ratio between the blue and red band was used to ~~determine the~~determine the existence of snow. However, the values vary and depend on the strength of shadows, therefore the thresholds were manually determined by an expert. To ensure the reliability of this approach, 500 random points in open terrain in 2019 were selected and manually checked regarding ~~to~~ their correct ~~snow-covered or snow-free~~ classification.

4.2.2 Outlier Mask

The outlier mask has the purpose to modify all unrealistic snow depth values, namely negative snow depths and~~, and~~ extremely high snow depths above 10 m ~~and~~to~~, to~~ No Data values. Only in the snow-rich~~y~~ year of 2019, ~~which was characterized by numerous extremely large avalanche depositions,~~ the upper limit was adapted to 15 m.

4.2.3 High vegetation mask

Due to uncertainties in the actual snow depth and problems with photogrammetric methods, areas with high vegetation were masked out~~Due to the uncertainties in the actual snow depth and problems with photogrammetric methods around high vegetation, these areas were masked out~~. H~~Pixels containing h~~igh vegetation, defined as vegetation with a height above 0.5 m, were identified through the vegetation classification and the calculated object height using the ALS point cloud. ~~High vegetation, defined as vegetation with a height above 0.5 m, only exists up to an elevation of approximately 2250 m in the region of Davos (Rixen et al. 2012). Correspondingly, the calculation of the high vegetation mask was also limited to this elevation.~~ Additionally, a generalis~~z~~ation of the high vegetation mask was required because wind, different sensor acquisition characteristics and the various capture times between ALS and Ultracam affected the extent of high ~~vegetation and therefore had an influence on the calculated snow depths. As tree density is dependent on elevation, the~~vegetation. The algorithm used for the generalis~~z~~ation differed between a rougher mask below 2050 m, where dense forests are predominant, and a finer mask above 2050 m, where free-standing trees and bushes are prevalent.

4.2.4 Water~~s~~ and glacier mask

The water~~s~~ and glacier mask prevents unrealistic snow depth values on water~~s~~ and glaciated areas. ~~The spectral characteristics of water often result in false classification as snow. Furthermore, d~~Due to low water levels during peak of winter, the actual height of snow (HS) on frozen lakes is underestimated. Therefore, larger lakes, rivers and dominant~~striking~~ streams were masked out. The data ~~river courses and shorelines of lakes were~~ was obtained from the Swisstopo TLM3D geodata (Federal Office of Topography swisstopo 2021c).

Another problem is the significant volume loss of glaciers (approximately 2 m per year) in recent years~~Another problem occurred on glaciated areas which are characterized by thickness losses (approximately 2 m per year) in recent years~~

(GLAMOS - Glacier Monitoring Switzerland 2021). Accordingly, the calculated snow depths from 2017 to 2020 on glaciers are overestimated and therefore masked out~~Accordingly, the calculated snow depths from 2017 to 2020 on glaciers are overestimated. Therefore, glaciated areas (stand: 2016) were masked out~~ (Linsbauer et al. 2021).

4.2.5 Infrastructure and building mask

The infrastructure and building mask prevents distorted snow depths caused by buildings and by temporary or moveable objects. ~~Therefore~~Consequently, all buildings were completely ~~masked~~masked out~~,~~ and infrastructure was partially masked. The buildings were derived from the classified point cloud of the ALS. The locations of technical constructions and infrastructure such as streets were obtained by the Swisstopo database. Railways, funicular railways, sport facilities, parking lots, ~~and~~ all streets in settlement areas and main roads outside the settlements were masked out. Technical constructions like avalanche fences were also set to No Data.~~All masked pixels were generalized by a similar approach as used for the vegetation mask.~~ A very rough generali~~z~~sation was used within ~~crowded~~dense settlements such as Davos, Arosa, and Klosters, whereas a finer generali~~z~~sation was applied for areas beyond these settlements.

4.2.6 Masking Overview

Using all presented masks (Fig. 5) on the raw snow depth values resulted in the final snow depth maps. ~~-~~For the snow depth map 2020~~In total,~~ around 67 % of all pixels remained in the snow depth maps. ~~With~~ 28 % of the main study area~~ part~~ was masked out ~~of the pixels masked out corresponds~~as it belonged to high vegetation areas. ~~With~~ Only less than 1 % ~~(in 2018 – 2021),~~ of the pixels~~number~~ were masked out ~~of outliers~~as outlier~~ is considerably lower than outliers observed in~~ (Table 3; Fig. A2).

Table 3. Area [km²] and percentage [%] of various masks, outliers and remaining snow depth values for the 2020 snow depth map.~~ 2020~~

	Water~~s~~	**Glacier**	**Building & infrastructure**	**High vegetation**	**Outlier**	**Snow depth values**
Area [km²]	1.1~~2~~	2.7~~9~~	6.6~~0~~	60.6~~7.2~~	1.7~~9~~	161.3~~0.8~~
Percentage [%]	0.5	1.2	2.7~~5~~	25.9~~28.0~~	0.7~~8~~	69~~7~~.0

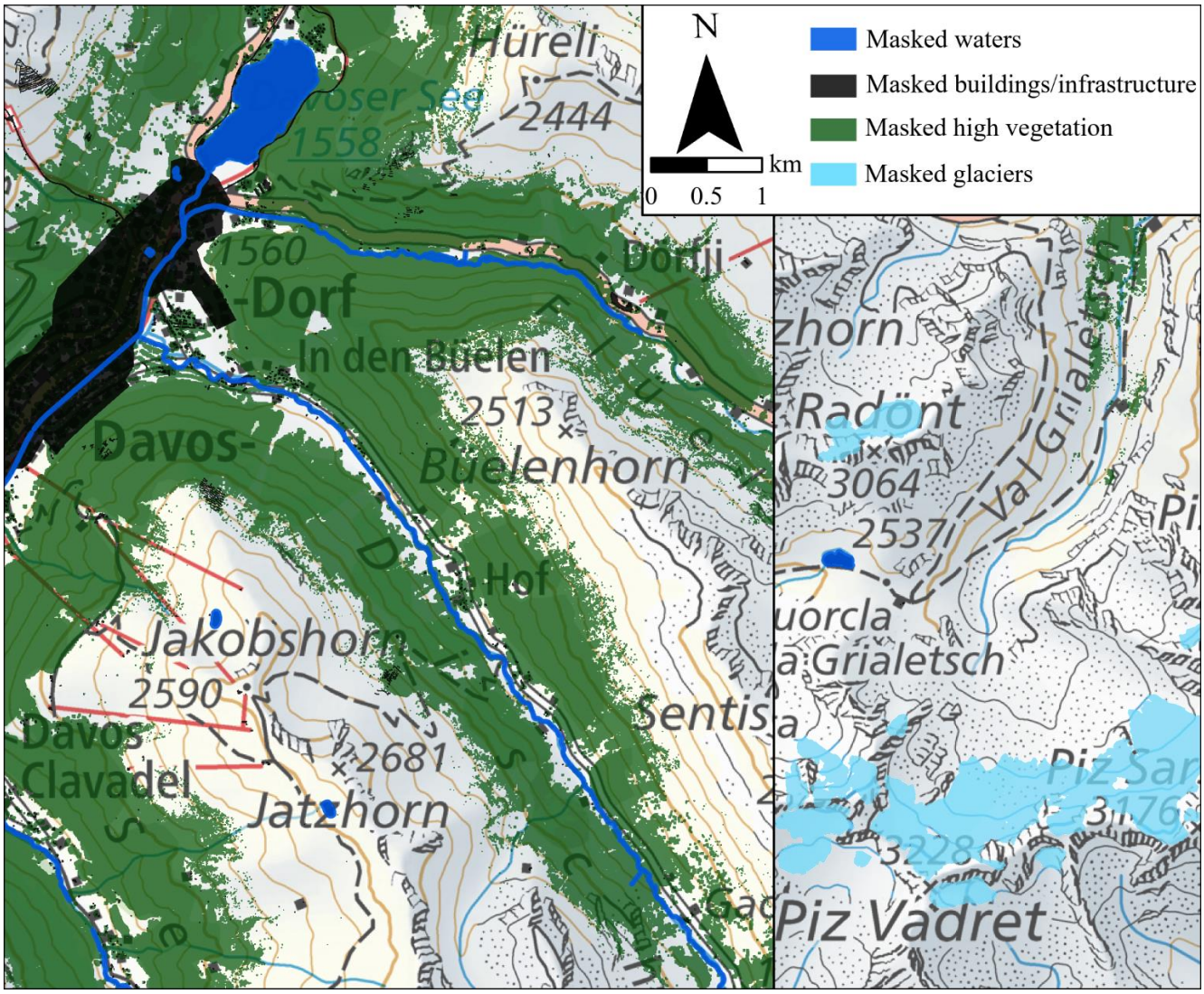

Figure 5. Spatial distribution of the masks used in selected extents of the main study area. Darkblue (water~~s~~), light blue (glaciers), green (high vegetation) and black (buildings and infrastructure) polygons symbolize the different masks. Rivers are overrepresented for a better identification (map source: Federal Office of Topography).

4.3 Accuracy Assessment

An essential part of this study is an extensive accuracy assessment of the snow depth values. Due to the absence of spatially continuous ground truth datasets, we ~~could only determine~~ determined the accuracy compared to several available reference datasets. ~~Basically, only a simultaneously recorded ALS would be able to provide accurate reference data on large scale, however, this, in turn, would lead to extremely high costs.~~ T~~herefore, t~~he accuracy assessment consists of five different methods which enabled a conclusive and spatially continuous evaluation of the annual winter-DSMs. The selected quality

procedures ~~for each~~differ between the years and depend on the availability ~~and the reliable implementation~~ of reliable~~e~~ reference data (Table 4).

- The first method ~~is to~~ uses independent **check points (M1)** as validation (Sanz-Ablanedo et al. 2018). Even though, the number of check points was limited, and they were predominantly not well-distributed over the entire study area, they are ~~an of check points was limited and they were predominantly not well-distributed over the entire study area, they are an~~ important indicator for the correct orientation of the winter-DSMs.
- Due to their outstanding accuracy, **UAS-derived DSMs (M2)** serve as ground reference and enabled direct and spatial comparison with Ultracam data over a small area (Deschamps-Berger et al. 2020; Marti et al. 2016).
- **Visual checks (M3)** by an expert examined the plausibility of calculated snow depths and the correct application of the masks over the entire study area.
- Comparisons of snow-free areas ~~of~~ on the winter-DSMs with the reference ALS exhibited further ~~possibilities for~~ evaluations. **Method 4 (M4)** determined deviations on the **main roads** beyond settlements which were always snow-free (Fig. 6). Extreme outliers exceeding 3 m (approximately MBE ± 4 SD) were excluded, because bridges, tunnels and moveable objects led to higher deviations.

  M4 was applied in most of the snow depth maps, except 2019. In 2019, the absence of the NIR-band in combination ~~to~~ with ~~occurring~~ puddles on the streets resulted in high deviations, which do not correspond to the actual accuracy. For a significant assessment, streets without puddles were manually digitalized and used as M4 in 2019.
- **Method 5 (M5)** considered deviations of **all other snow-free pixels (M5)** beyond settlements compared to the ALS-DTM. Pixels with vegetation heights exceeding 0.05 m ~~(derived from normalized ALS DSM)~~ were excluded. ~~This procedure allowed an accuracy assessment of numerous~~

Table 4. Overview of the accuracy assessment methods performed in the different years.

	2017	2018	2019	2020	2021
M1: Check Points	×	✓	(✓)	✓	✓
M2: UAS	×	✓	×	×	✓
M3: Visual check	✓	✓	✓	✓	✓
M4: Comparison ALS on streets	✓	✓	(✓)	✓	✓
M5: Comparison ALS beyond streets	✓	×	×	✓	✓

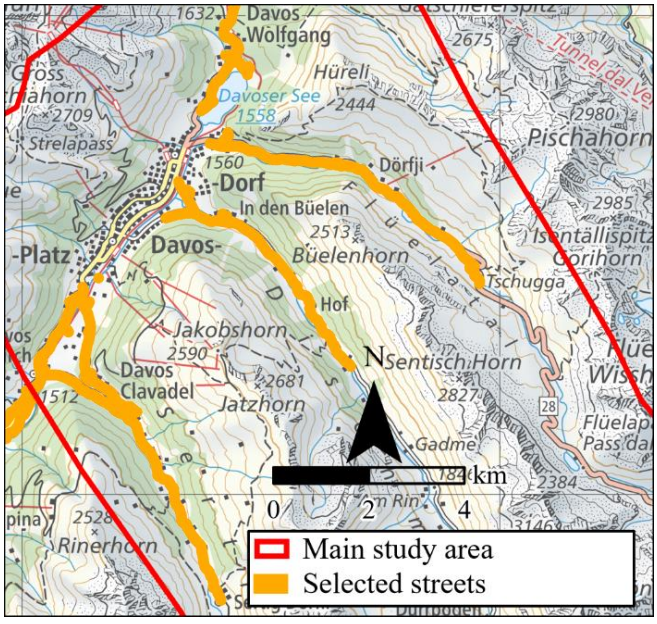

Figure 6. Overview roads used (orange lines) for the accuracy assessment method 4, lines are overrepresented for better identification (map source: Federal Office of Topography).

~~pixels in the entire study area. The identification of snow-free pixels is based on the snow mask. Despite a the high exactness accuracy of this method, some falsely classified pixels (e.g snow mixed with soil) appeared in each snow mask.~~ Moreover, occasional and temporal changes of objects and infrastructure occurred between the acquisitions of the winter DSMs and the ALS. Therefore, extreme outliers exceeding 3 m (approximately MBE ± 4 SD) were excluded. Limited snow-free areas beyond streets in the winters of 2018 and 2019 impeded a meaningful evaluation of~~n~~ snow-free pixels in these years.

The quantitative procedures were evaluated by various commonly~~-~~used statistical quality grades such as mean bias error (MBE), standard deviation (SD), RMSE, median (MdBe) and normalized median absolute deviation (NMAD) (details in ~~;~~ Eberhard et al. 2021 and in Höhle und Höhle 2009). The significant impact of a ~~-~~few pixels with high deviations caused by the distortions described above led to the calculation of quality grades, excluding deviations beyond the confidence interval (MBE +- 2 SD).~~makes an additional filtering of the deviations necessary. This approach excluded all deviations beyond the confidence interval (MBE ± 2 SD) and was applied for the accuracy assessments of the ALS and the UAS.~~

Finally, since the accuracy of the snow depth values ~~is~~ also dependents on the ~~exactness of the~~ **reference ALS-DTM**, we have examined the specified accuracy (Z = 0.1 m) comparing~~. Therefore, we compared~~ 24 reference points (see section 3.2.3) on snow-free areas with the ALS-DTM.

5 Results and validation

5.1 Accuracy Assessment

The quantitative part (M1, M2, M4~~3~~, M5~~4~~) of the accuracy assessment compares the deviations of the winter-DSM to a selected reference dataset~~of the accuracy assessment evaluates the deviations of the winter-DSMs to with a selected reference dataset~~. Due to the horizontal accuracy of the check points (M1) of the winter-DSMs was approximately 0.1 m in each year, which is also influenced by inaccuracies of the GNSS, we especially focused on the vertical accuracy. The RMSE value comparing the ALS-DTM to 24 reference points of 0.03 m demonstrates the high reliability of the reference ALS. The achieved accuracy of the reference-DSMs derived from UAS was identified by using check points with a RMSE of 0.06 m (2021) and 0.1 m (2018).

5.1.1 2017

The accuracy assessment of the winter-DSM 2017 calculates RMSE values of 0.26 m on open streets and 0.3 m on snow-free pixels after outlier removal (MBE ± 2SD) (Table 5). Resulting dispersions of method 4 (SD = 0.33 m, NMAD =0.28)

and method 5 (SD = 0.42 m, NMAD =0.32) have considerably higher values compared to the other years~~, which show the lower reliability of this winter-DSM based on the precursor sensor Vexcel Ultracam X~~ (see section 3.1; Table 1). The same result can be clearly seen at the significantly larger interquartile range of the winter-DSM in 2017 in Fig. 10. Additionally, Fig. 7 shows the difference of the accuracy and the ~~-~~corresponding dispersion between Ultracam X and the successor Ultracam Eagle M3. The impact of the higher deviations is evident regarding the high number of outliers (3%; negative snow depths) in steep ~~number of outliers (negative snow depths) in complex~~ and heterogenous terrain. Furthermore, inaccuracies of the NIR-band led to insufficient classification of the snow masks.

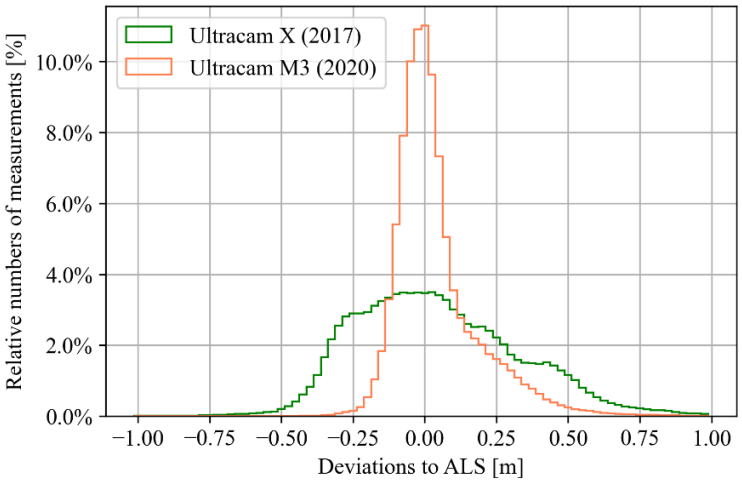

Figure 7. Comparison of the dispersion of deviations on streets to ALS between Ultracam X (green, 2017) and Ultracam Eagle M3 (light red, 2020).

Accordingly, numerous pixels on streets, in transition zones of snow-free to snow-covered and in shaded areas are falsely classified as no snow.

5.1.2 2018

In 2018, large cloud-covered areas were excluded from the processing. Therefore, missing images and partly cloud-covered images caused less overlap in these regions ~~and complicated the processing of the remaining study area~~. Nevertheless, the deviations of the ten check points (RMSE 0.13 m) and the comparison with the UAS-derived DSM (RAW = 0.12, Filtered = 0.09 m) demonstrate a very high ~~high~~ accuracy of the winter-DSM (Table 5). The low aspect-dependency of the deviations between UAS and Ultracam (Fig. 8) can be explained by the ~~four days~~ delay in capture time and therefore compression of the snowpack on

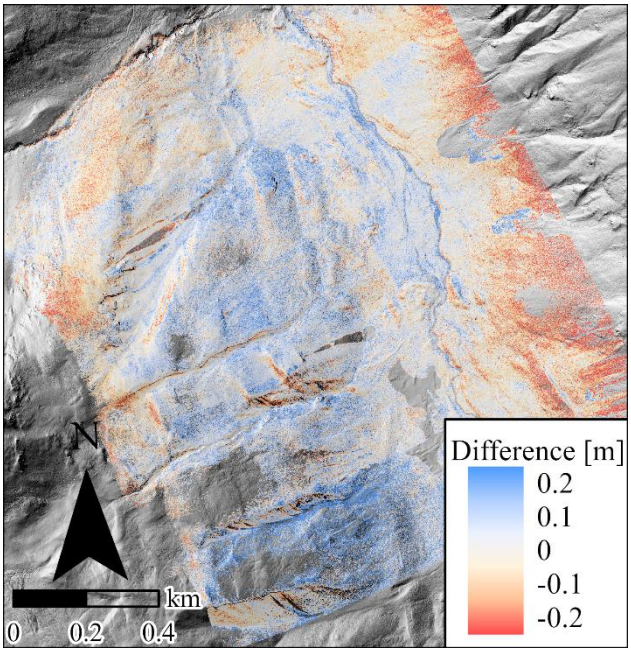

Figure 8. Difference calculation of the DSMs around the Schürliaalp derived from Ultracam data and UAS in 2018.

southern slopes due to mild temperatures and strong solar radiation. ~~However, the clouds caused slight regional inaccuracies of the snow depths.~~ The median of method 4 (RAW = 0.08, Filtered = 0.09) shows a slight overestimation of the snow depths, which especially occurred ~~in the~~ south of Davos, close to cloud-covered areas. Despite these overestimations, the RMSE (RAW = 0.18, Filtered = 0.16) of the deviations on roads also proves the spatially very high reliability of the winter-DSM. ~~In addition, the height of the winter-DSM in high mountain regions in the southwest and also close to cloud-covered regions are slightly underestimated by 0.05 to 0.1 m. These underestimations caused a few negative snow depths on pixels covered by a thin snowpack in extremely steep areas.~~ The classification of snow-covered pixels worked reliable, only isolated pixels in wet snow avalanches, exhibiting a snow-soil mixture, were falsely classified. ~~The classification of snow-covered pixels worked satisfyingly, whereby separate pixels of sprinkled snow or snow mixed with soil of wet snow avalanches are still falsely classified.~~

5.1.3 2019

The occurrence of technical errors on the airplane prevented the capture of the NIR-band, which can decrease the successful reconstruction of low-contrast snow surfaces and accordingly the accuracy of the DSM ~~which can decrease the successful reconstruction of low-contrast snow surfaces and then, accordingly, also the accuracy of the DSM~~. However, no significant influence on the reconstruction or accuracy of the DSM was determined. ~~However, except from selected areas in north faces, no significant influence on the reconstruction or accuracy of the DSM was determined.~~ This ~~statement~~ high accuracy is confirmed by evaluations of the RMSE of the check points (0.07 m) and especially the RMSE of the

manually digitalized snow-free areas (Filtered = 0.11 m) (Table 5; Fig. 10). ~~Below the treeline, the height of the winter-DSM was slightly overestimated by 0.05 m.~~ Using the snow~~-~~ mask~~,~~ ~~based on manually determined thresholds,~~ also led to a high-quality grade of more than 99 % correctly classified pixels (method described in section 4.2.1). ~~The method used only had issues in snow mixed with soil, on frozen rocks and in extremely tracked areas.~~

5.1.4 2020

The capture of the aerial images in 2020 was characteri~~s~~~~z~~ed by perfect acquisition conditions ~~during the Ultracam flight~~. Consequently, the winter-DSM in 2020 evince a very ~~very~~ high accuracy of around 0.1 to 0.15 m~~.~~ ~~This accuracy was~~ determined by the use of 36~~a high number of~~ well-distributed check points, which show a RMSE of 0.07 m (Table 5). The RMSE values of method 4 also indicate a ~~similarly~~ high accuracy (RAW = 0.19, Filtered = 0.13). Furthermore, the large snow-free areas in 2020 enable a representative accuracy assessment of method 5 which considers deviations in different elevations and slopes. The RMSE of ~~the M5?~~ filtered deviations (0.18 m) in combination with the NMAD (0.16 m) of method 5 shows the high reliability of the winter-DSM in the entire study area ~~and also~~and in steep~~complex~~ terrain. The deviations of M5 in extremely steep areas exceeding 40° (Filtered RMSE = 0.3 m) confirmed, that the ~~inaccuracies~~ quality of the winter-DSM ~~i~~de~~n~~creases with ~~rising~~ increasing steepness, but is still high (Bühler et al. 2015; Meyer et al. 2022).

5.1.5 2021

In 2021, the surface above ~~around~~ 1800 m a.s.l. was covered by a new snow layer, which caused less contrast during the Ultracam recording. Despite~~,~~ these difficult conditions, the check points indicate a similar~~ly~~ high accuracy ~~like~~ as in 2020 (RMSE = 0.12 m). The RMSE (RAW = 0.14, Filtered = 0.12) values of the comparison between the DSMs derived from Ultracam and UAS also show very good ~~satisfying~~ results, with a slight tendency to underestimate~~s~~ the winter-DSM (Fig. 9). The underestimation is characteri~~s~~~~z~~ed by a negative median (Filtered = -0.09). The median values of method 4 (RAW and Filtered =0~~, Filtered = 0~~) and method 5 (RAW ~~,~~and ~~Filtered~~Filtered = 0) ~~indicate h~~show however, that this underestimation is a local problem and not valid for the entire study area. The ~~low~~ RMSE value calculated with method 4 (Filtered = 0.11 m) and 5 (Filtered = 0.16 m) demonstrates the very high accuracy of the snow depths

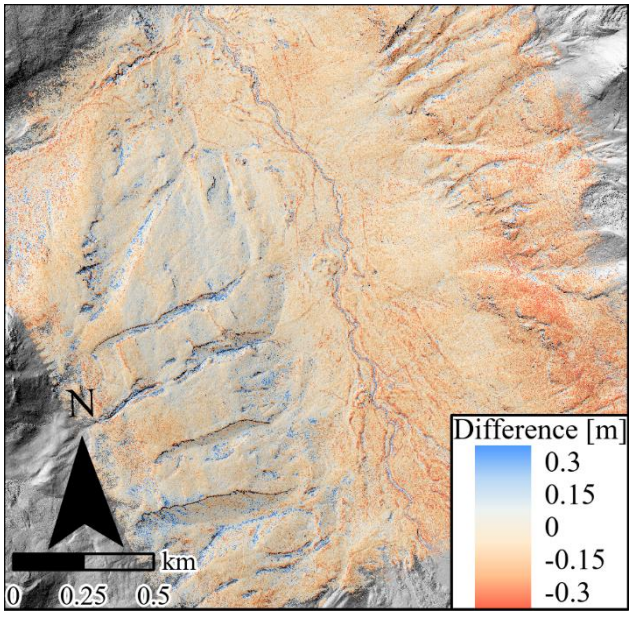

Figure 9. Difference calculation of the DSMs around the Schürliaalp derived from Ultracam data and UAS in 2021.

(Table 5). Additionally, partly cloud-covered areas led to no significant increase of the dispersion, which is shown in the low NMAD values of method 4 (RAW = 0.09) and method 5 (RAW = 0.15).

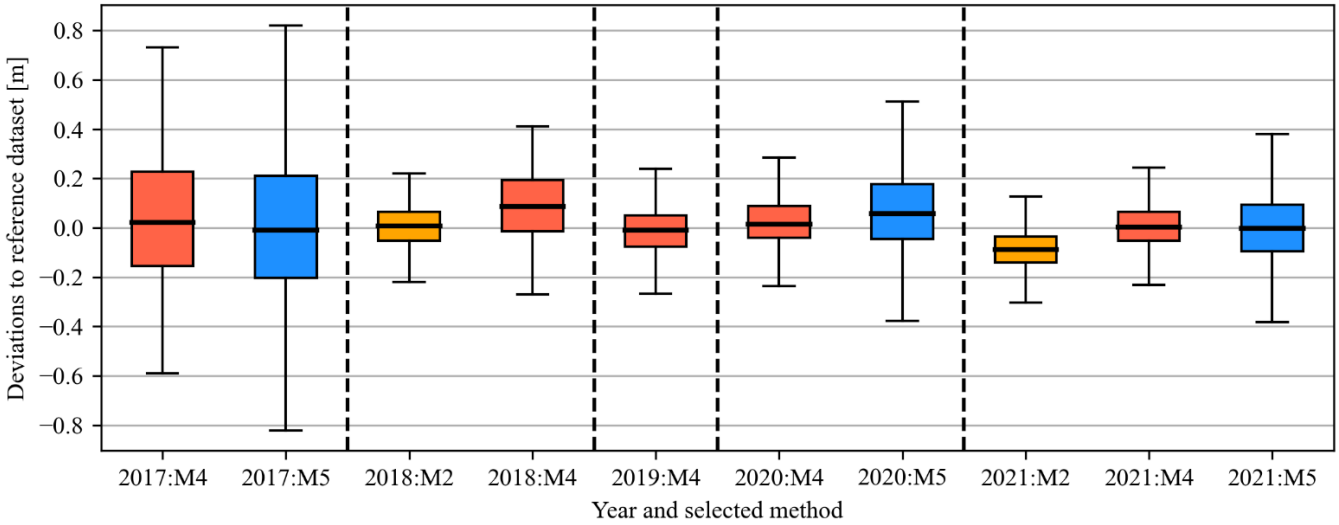

Figure 10. Box plots of the filtered deviations (MBE ± 2SD). Used Methods: M2 (orange), M4 (red) and M5 (blue) for each year.

Table 5. Overview and comparisons of the quality grades of the winter-DSMs; Column "Filtered" excluded outliers (MBE ± 2 SD).

		M1: Check Points	**M2: UAS**		**M4: Comparison ALS (streets)**		**M5: Comparison ALS (snow-free pixels)**	
		RAW	**RAW**	**Filtered**	**RAW**	**Filtered**	**RAW**	**Filtered**
2017	MBE[m]	×	×	×	0.07	0.045	-0.02	0
	SD[m]	×	×	×	0.33	0.26	0.42	0.3
	RMSE[m]	×	×	×	**0.33**	**0.26**	**0.42**	**0.3**
	MdBE [m]	×	×	×	0.03	0.02	-0.02	0
	NMAD [m]	×	×	×	0.28	0.28	0.32	0.3
	Number measurements	×	×	×	347'068	336'135	15'003'508	14'355'536
2018	MBE[m]	×	0	0	0.07	0.08	×	×
	SD[m]	×	0.12	0.09	0.16	0.14	×	×
	RMSE[m]	**0.13**	**0.12**	**0.09**	**0.18**	**0.16**	×	×
	MdBE [m]	×	0	0	0.08	0.09	×	×
	NMAD [m]	×	0.09	0.09	0.16	0.15	×	×
	Number measurements	10	7'471'650	6'949'690	132'558	127'191	×	×
2019	MBE[m]	×	×	×	×	0	×	×
	SD[m]	×	×	×	×	0.11	×	×
	RMSE[m]	**0.07**	×	×	×	**0.11**	×	×
	MdBE [m]	×	×	×	×	0	×	×
	NMAD [m]	×	×	×	×	0.09	×	×
	Number measurements	6	×	×	×	25'944	×	×
2020	MBE[m]	×	×	×	0.06	0.04	0.09	0.07
	SD[m]	×	×	×	0.18	0.12	0.27	0.17
	RMSE[m]	**0.07**	×	×	**0.19**	**0.13**	**0.28**	**0.18**
	MdBE [m]	×	×	×	0.02	0.02	0.07	0.06
	NMAD [m]	×	×	×	0.10	0.09	0.17	0.16
	Number measurements	40	×	×	221'087	214'114	30'933'482	29'522'927
2021	MBE[m]	×	-0.08	-0.08	0.03	0.01	0.02	0
	SD[m]	×	0.12	0.08	0.18	0.11	0.27	0.16
	RMSE[m]	**0.12**	**0.14**	**0.12**	**0.19**	**0.11**	**0.26**	**0.16**
	MdBE [m]	×	-0.09	-0.09	0	0	0	0
	NMAD [m]	×	0.08	0.08	0.09	0.09	0.15	0.14
	Number measurements	19	16'386'474	15'987'661	227'907	217'453	6'342'785	6'141'131

565

5.2 Snow depth maps

Despite varying and partly difficult~~different and complexdifficultcomplex~~ acquisition conditions (section 3.1) as well as some extremely steep and complex areas, on average, more than 99 % of the snow depth values in ~~the requested and~~ not ~~-~~masked areas were reconstructed. Only in the winter-DSM from 2017, the image matching failed in few overexposed or shaded regions~~, due to poorer radiometric characteristics of the sensor Vexcel Ultracam X.~~ The high rate of success enabled the spatially continuous snow depth mapping of open areas ~~the region~~ around Davos. The spatial resolution of the maps (0.5 m) and the orthophotos (0.25 m) provide an excellent overview of the snow depth distribution within the study area. The existing level of detail shows numerous small-scale features over ~~such~~ a large area and demonstrates the high variability of snow depths even within small distances. Special characteristics of the study area are the strongly varying average snow depths and snow cover. The average snow depth values of the selected ~~-~~ years ranged from 1.29 m in 2017 to 2.36 m in 2019 (Table 6). ~~–~~Comparing the 2019 and 2020 snow depth maps, significant differences in snow depth distribution and related features can be seen ~~In particular the comparison of the snow depth maps from 2019 and 2020 is suitable to visualize visualise significant differences of the snow depth distribution and related features~~ (Fig. 11). ~~When exemplarily comparing 2019 with 2020, we found that i~~In 2019, the study area was almost completely snow-covered, exhibited numerous regions with high snow depths exceeding 3 m and was ~~characterized~~ characterised by the ~~occurence~~occurrence of many slab avalanches. In contrast ~~to that~~, the average snow depth in 2020 was considerably lower (1.42 m). ~~with a mean value of 1.42 m,~~ The area was often ~~characterized~~ characterised by ~~often~~ snow-free slopes below 2400 m a.s.l. in southern aspects as well as numerous glide-snow and wet-snow avalanches. ~~In general, for 2020, t~~Furthermore, t~~T~~he aspect-dependence of the snow depths~~HS~~ was more decisive in 2020 than in 2019.

~~However, d~~Despite the high difference of the average snow depth values between these two years, similar patterns ~~regarding~~in the relative snow depth distribution and occurrence of special features are identifiable. In general, the snow depths~~HS~~ in both years increases with rising elevation until a certain level close to ridges or peaks. Higher snow depths are more frequently found on northern aspects compared to south-facing slopes which shows the aspect-dependence of snow depths. Furthermore, higher and lower relative snow depths of both snow depth maps occurred at similar locations (Fig. 11).

Table 6. Overview average snow depths [m] and standard deviation [m] of each annual snow depth map.

Year	2017	2018	2019	2020	2021	Mean
Average	1.29	1.50	2.36	1.42	1.71	1.66
SD	0.87	0.83	1.33	1.01	1.11	1.03

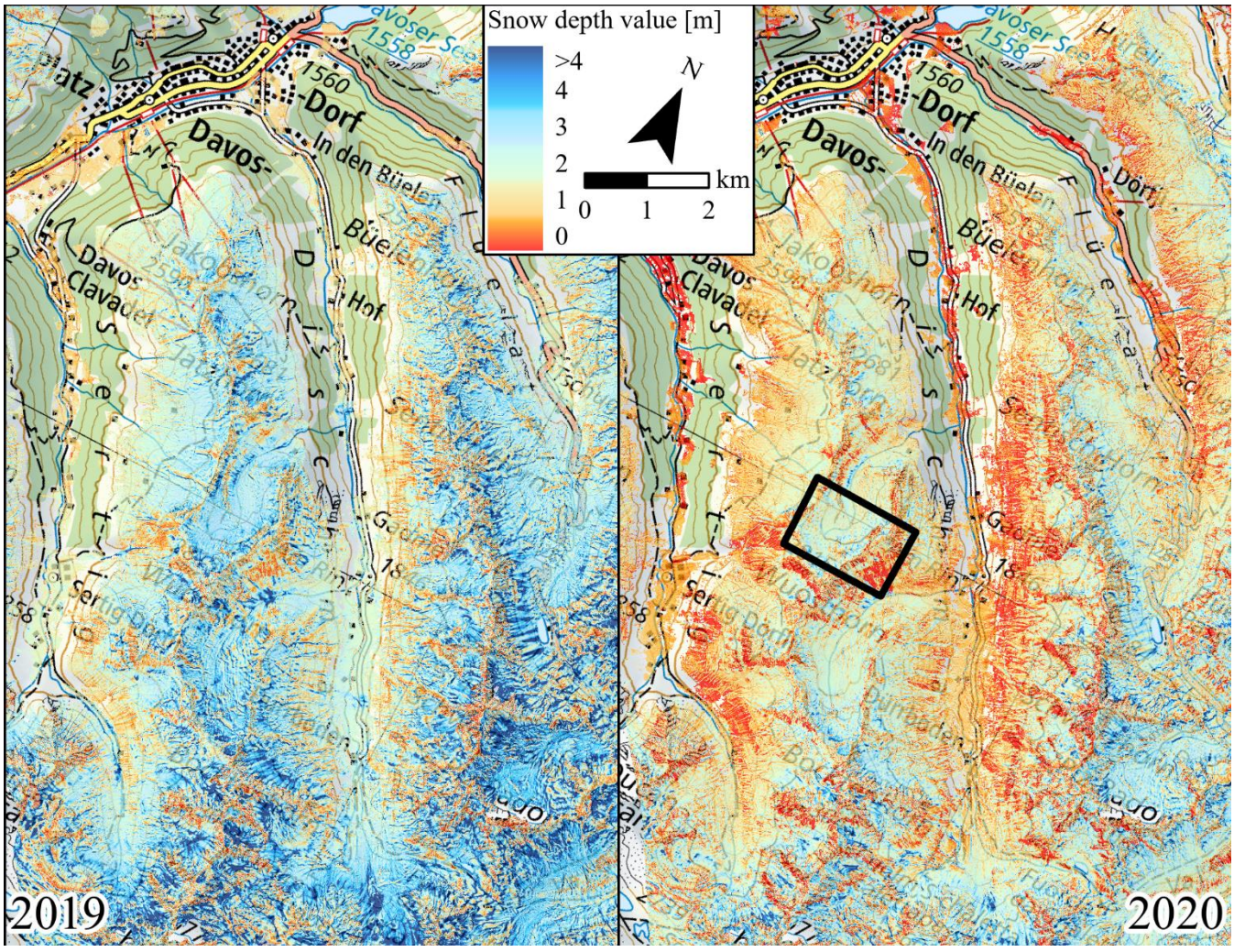

Figure 11. Comparison of an extent of snow depth maps from 2019 and 2020 during corresponding peak of winter. The black polygon shows the location of the selected small catchment for a more detailed comparison between the available snow depth maps (Fig. 12) (map source: Federal Office of Topography).

We further investigated the snow distribution patterns ~~between the years~~ by ~~looking at~~comparing the relative snow depth distribution between the years. The normali~~z~~zed snow depth values of each year were calculated by the relation of the HS in contrast to the average snow depth of the selected area in the corresponding year. ~~In comparison to the absolute snow depth maps, t~~The normalized snow depth maps have the advantage of being independent from differences in the ~~average~~ absolute snow depth between the years, which enables a better overview of the actual snow depth distribution. As depicted exemplarily in Fig. 12, we observed similar distribution patterns ~~for the distribution~~ between all years. Generally, higher relative snow depths often occurred at deposition zones of avalanches, along terrain edges in wind-protected zones and within sinks~~.~~, L~~l~~ower snow depths were frequently observed on slopes exceeding 35°, in wind~~-~~exposed areas and in the release zones of avalanches

(see also 6.2.3~~.~~). However, a few features such as ~~selected~~ avalanches ~~only arose in~~ in certain tracks only occurred in ~~separated~~ some years.

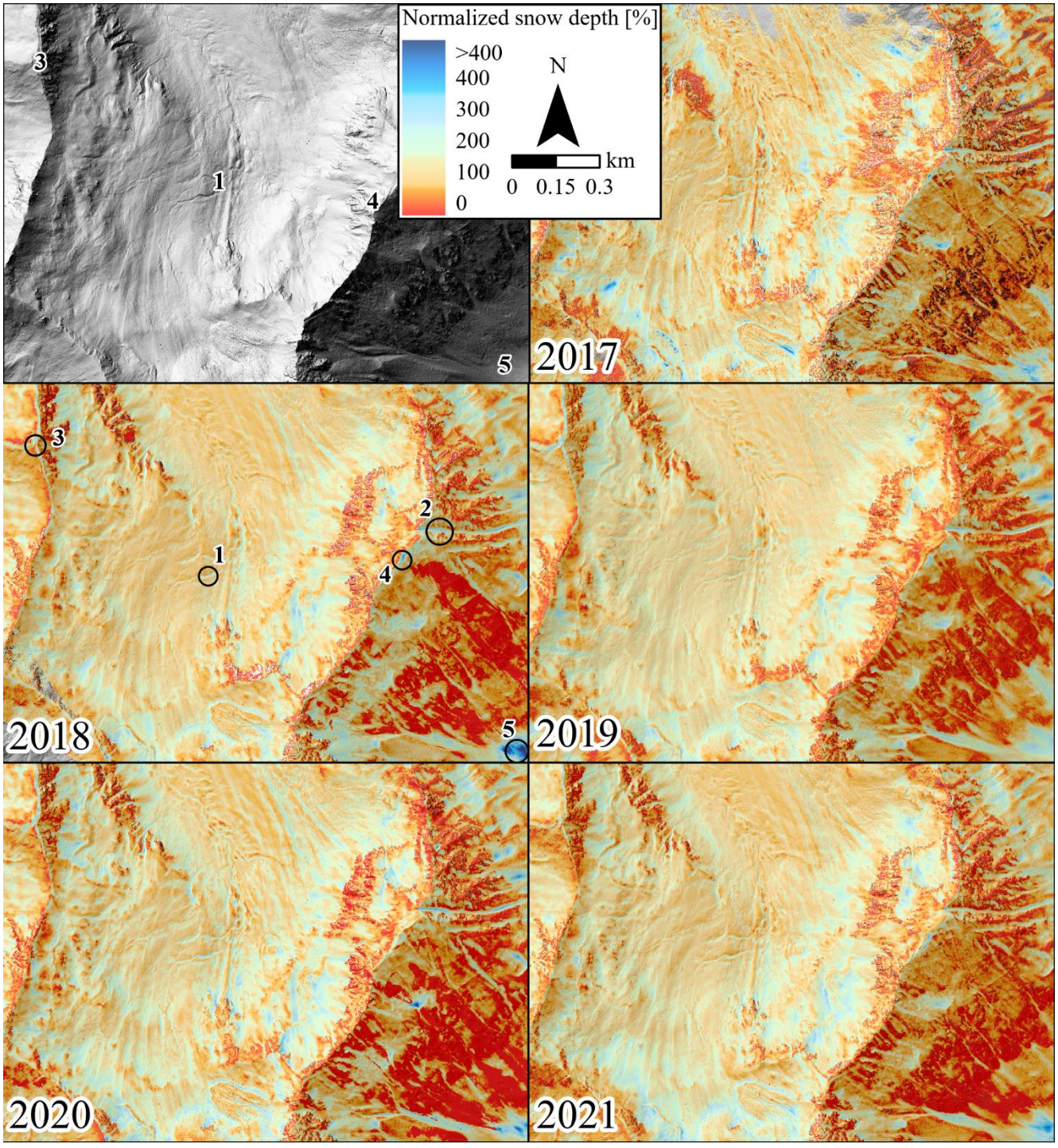

Figure 12. Comparis~~i~~on of the normalized snow depth maps of the 5-year period (2017 – 2021) during peak of winter in a small cat~~a~~chment (3 km²) close to Börterhorn. Numbers in the hillshade locate different special features, which demonstrate the existing grade of detail: 1. Filled small ~~brooks~~creeks; 2. Filled drainages in an extremely steep area close to Börterhorn; 3. ~~Conspicous~~ remarkable cornice between Tällifurgga and Witihüreli; 4. Cornice between Wuosthorn and the Börterhorn; 5. Deposition zone of avalanches.

~~Subsequently, we investigated the occurrence of further additional special features in the entire study area.~~ The detailed detection of numerous avalanches by means of the snow depth maps and corresponding orthophotos is a salient characteristic of the data. In particular, glide-snow avalanches, striking slab-avalanches and deposition zones of wet-snow avalanches can be identified. The investigation of the snow depth distribution around the fracture line enables the calculation of the release height. Exemplary shown in Figure 13, the release height of this slab avalanche was approximately 0.95 m.~~, which enablinges further research on the avalanche activitiesy and characteristics of the corresponding period (Fig. 13).~~

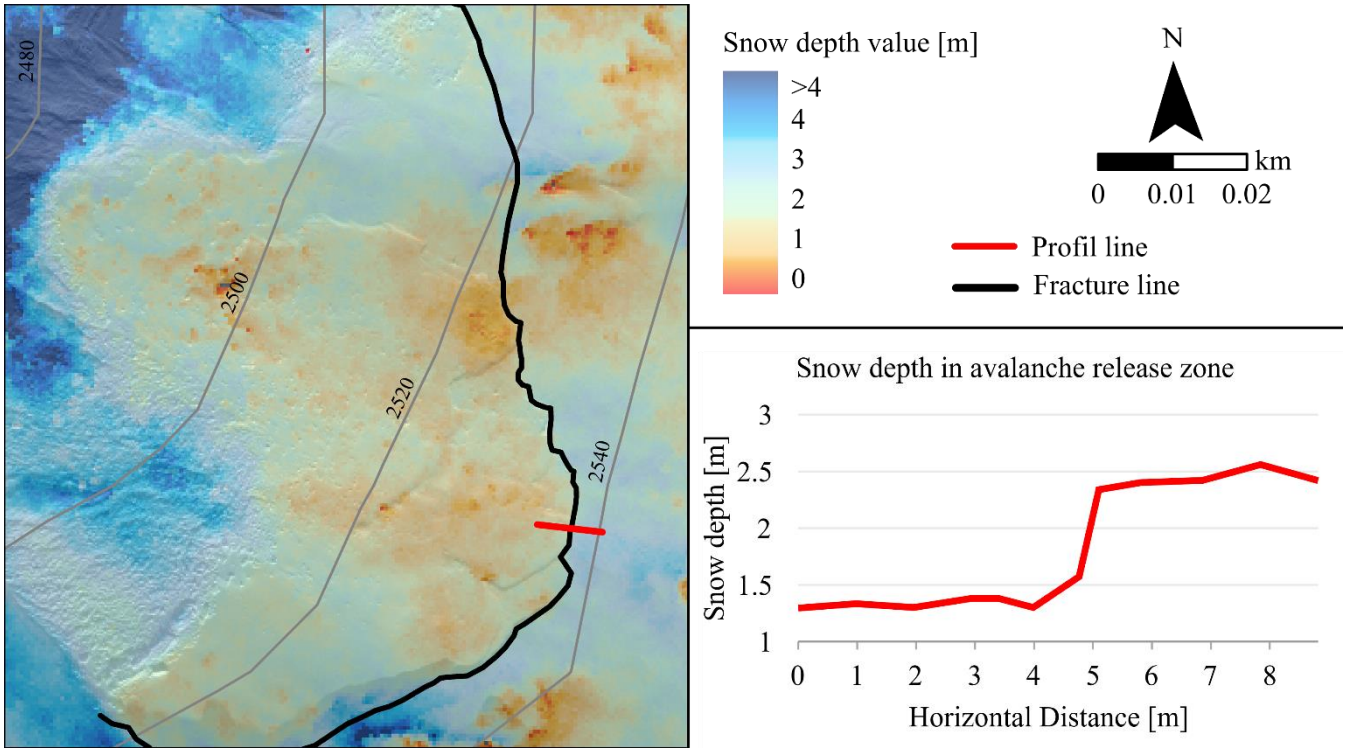

Figure 13. Overview of the snow depth distribution of the ~~a~~ release zone of a slab-avalanche close to the Börterhorn (Dischma Valley) captured by the Ultracam in 2019; red line symboli~~z~~es a height profile ~~which~~ showing~~s~~ the course of snow depth values vertical to the fracture line; the prominent difference ~~of~~ in ~~the~~ snow depths indicates the release height of around 0.95 m.

To present additional applications of our snow depth maps, we ~~thoroughly~~exemplarily assessed snow depth distribution around different avalanche protection structures~~In addition, we looked in detail on the snow depth distribution around different protective constructions such as avalanche fences to present other applications of our snow depth maps~~. Therefore, the workflow was slightly adapted by unmasking the avalanche fences~~To investigate the snow depths between the avalanche fences, the workflow used was slightly adapted toby not masking out the avalanche fences~~. In 2019, the Ultracam recording was shortly after a large snowfall (1.3 m new snow at Weissfluhjoch within 7 days) during a snow-rich~~y~~ winter. The orthophoto and ~~the~~ corresponding snow depth map shows that large parts of the release-~~-~~zone avalanche fences, ~~in the~~ south of the ~~right~~ wind-drift snow fences (1), were completely buried ~~by~~ as snow accumulated ~~snow depths of~~ up to 6 m (Figure 14). The avalanche~~s~~ fences close to the ridge (2) were also covered by a prominent cornice with a snow height of 5.5 m.

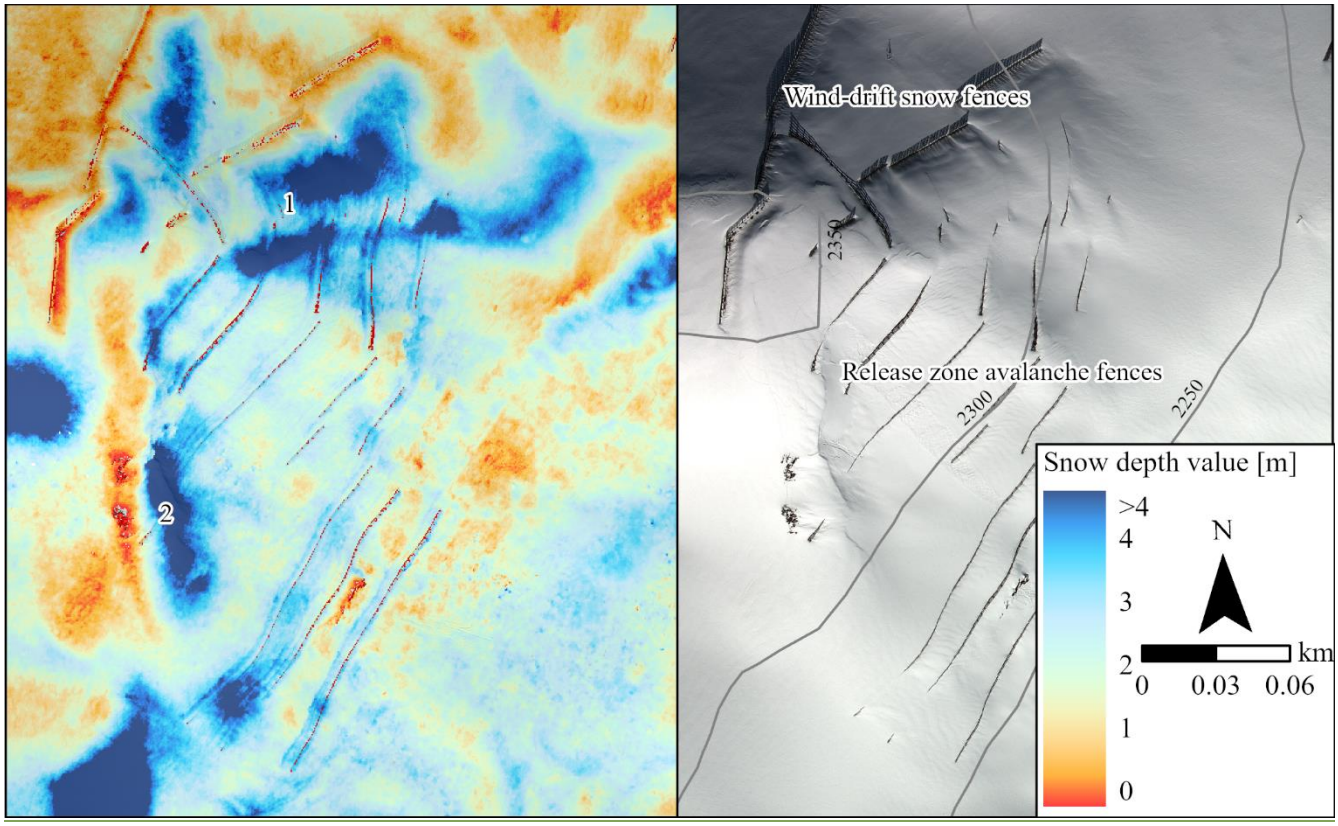

Figure 14. Snow depth distribution and corresponding orthophoto around different avalanches fences at the Grüneniberg captured by the Ultracam flight on the 16th March 2019. The numbers 1 and 2 symbolize buried avalanche fences with high snow depths exceeding 5 m.

We also compared the average snow depth value of the different snow depth maps (core area) with the punctual snow depth measurements from the eight AWS around Davos, which are well distributed at different elevations and aspects in our study area (Figure 1).

Despite the large differences in snow heights between the years, the average value of all AWS was similar to the average value (+/- 0.07 m on average) derived from our snow depth maps (). Only in 2018, when the main part of the higher mountains was cloud-covered, our value was considerably lower (- 0.22 m) compared to the mean of the snow depth measurements from AWS.

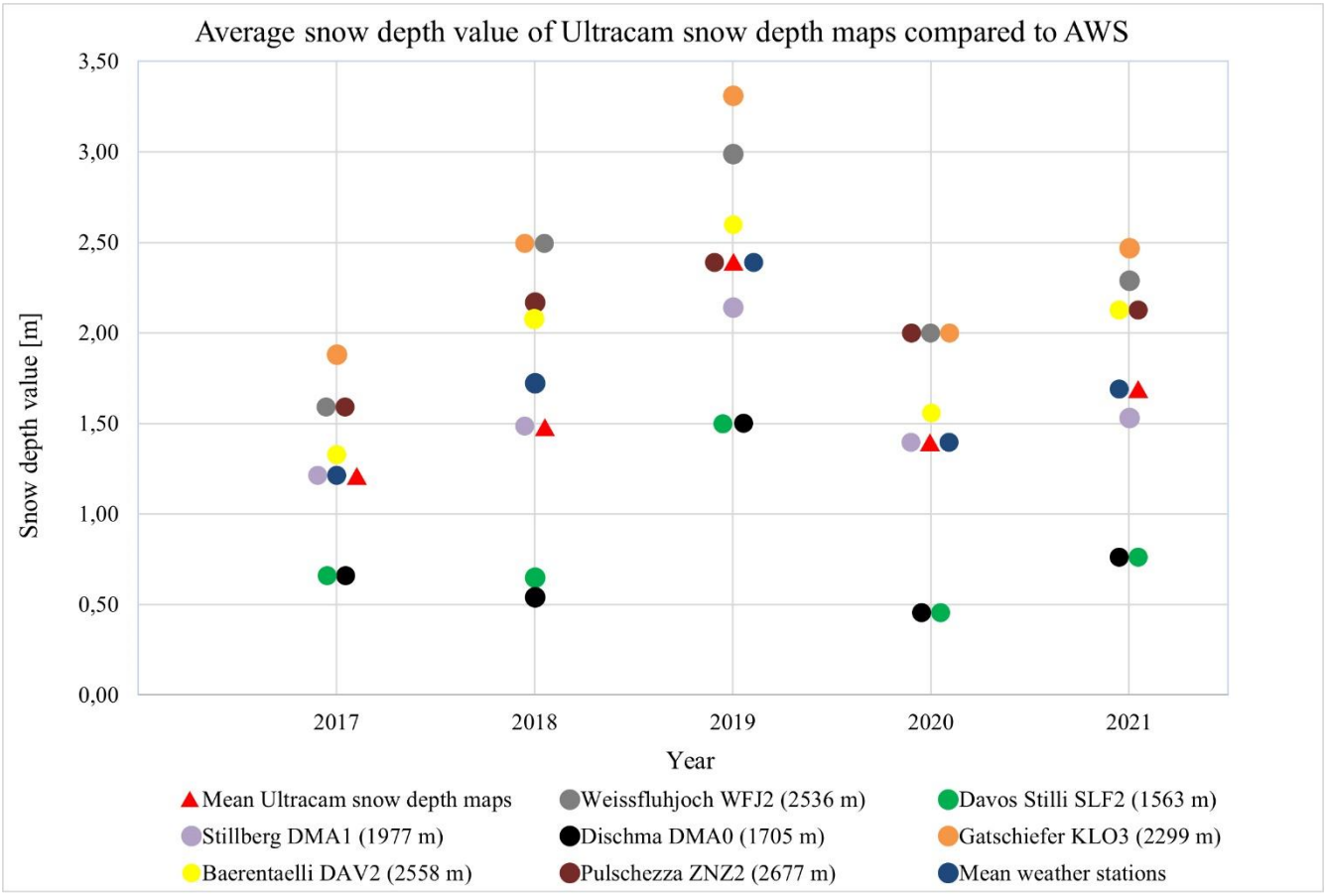

Figure 15. Average snow depth value from the Ultracam snow depth maps compared to snow depth measurements from automatic weather stations. Locations of the AWS are shown in Fig. 1

~~**Figure .** Average snow depth value of from the Ultracam snow depth maps compared to snow depth measurements of from automatic weather stations. Locations of the AWS are shown in **Fig. 1**.~~

AWS snow depth measurements ~~represent the~~are supposed to yield typical snow height ~~surrounding area~~. Hence, finding a suitable location for a new AWS ~~strongly depends on the snow depth distribution~~is a matter of finding an ideal location with ~~represetative~~representative snow height in ~~thearea~~the area of interest ~~in the corresponding area~~.~~Since the point snow depth measurement of the AWS represents the surrounding region, the finding of a suitable location of new AWS especially depends on the snow depth distribution in the corresponding area~~ .~~To~~ facilitate this ~~decision~~decision-making process~~To facilitate this finding process~~, ~~we implemented our snow depth maps in a model, developed by the~~ SLF developed a model, taking into account snow depth, to assess the suitability for a new station in the Dischma V~~v~~alley. Regarding the snow depth distribution, the model assesses the representativity of the measured snow depth ~~height~~ for the area (Figure 16). In addition, the model also considers different topography parameters such as roughness, avalanche danger (Bühler et al. 2022) and slope gradient.

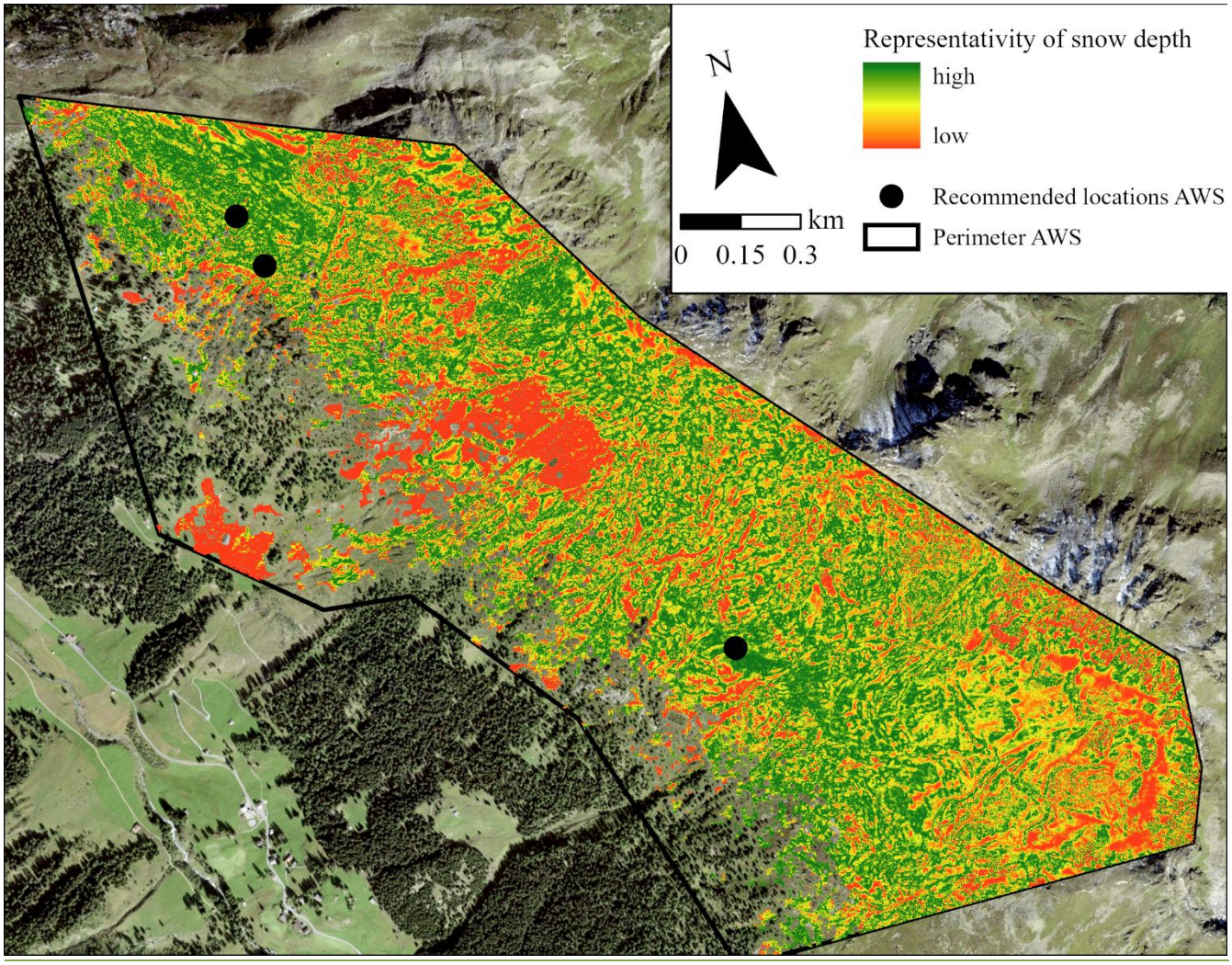

Figure 16. Representativity **of** punctual **snow depth** measurements (possible locations for AWS) for the entire perimeter (black polygon) derived from airplane snow depth maps. Black circles symbolise in the field predefined locations for the AWS. The south location was selected due to its high representativity (dark green), low avalanche danger and flat terrain for the new AWS Lukschalp (map source: Federal Office of Topography).

~~**Figure . Suitability map for finding of the location for** an **AWS** location **in the Dischma valley.**~~

6 Discussion

In this study we processed the data ~~of~~ from the annual Ultracam flights ~~from~~ (2017 to 2021) to snow depth maps. We investigated the necessary processing steps to derive accurate winter-DSMs, to ~~create and~~ apply required masks and to assess

the characteristics of the resulting snow depth maps. We analysed the accuracy and validity of the resulting winter-DSMs and used the snow depth maps for different applications~~with the help of an accuracy assessment~~. In this section, we discuss the obtained results.

6.1 Processing of snow depth maps

This study focussed on the accurate and consistent processing of large-scale snow depth maps under different acquisition conditions with the new Vexcel Ultracam sensors over a period of five years. We have ~~ascertained~~observed a significant quality increase from the Vexcel Ultracam X to the successor Eagle M3 due to its ~~better~~higher GSD ~~using the same flight altitude~~ and better radiometric characteristics. Data from the Ultracam X in 2017 exhibited errors in the NIR-band, which complicated the classification of snow-free pixels. T~~Additionally, t~~he RGB-sensor of the Ultracam X was partly overexposed, hence Agisoft Metashape had problems to find matching points in few ~~sunny~~ sunlit snow areas. The accuracy assessment in 2017 ~~also~~ shows that the RMSE (~ 0.25 m) of the winter-DSM~~, with around 0.25 m,~~ is significantly poorer than in the following years (Table 5; Fig. 10), which is no noticeable~~y~~ advance compared to other studies (Bühler et al. 2015; Nolan et al. 2015).

With the new ~~Ultracam~~ Vexcel Ultracam Eagle M3 sensor, Agisoft Metashape was able to reconstruct almost the complete surface, even in heavily shaded areas, on surfaces covered by fresh snow as well as in partly cloud-covered regions. A similar successful processing of small catchments was achieved by Meyer und Skiles (2019). However, our approach still reveals a significant progress in photogrammetric snow depth mapping compared to other large-scale snow depth maps from previous studies (Bühler et al. 2015; Nolan et al. 2015). ~~Only in completely cloud-covered areas, Agisoft Metashape had problems to reproduce the entire surface. This successful processing was already shown for small catchments (Meyer und Skiles 2019) , but is a significant progress for photogrammetric snow depth mapping compared to large-scale snow depth maps from previous studies (Bühler et al. 2015; Nolan et al. 2015).~~ Using the Ultracam Eagle M3 also resulted in a considerable better GSD under similar flight altitudes compared to ~~current~~ recent studies (Meyer et al. 2022) ~~(~~Meyer et al. 2021). The better GSD enables the exact processing of snow depth maps with a spatial resolution of 0.5 m, which is better than previous large-scale snow depth maps and required to capture small scale distribution pattern accurately (Miller et al. 2022). ~~The better GSD enables the exact processing of snow depth maps with a spatial resolution of 0.5 m., which resulted in a better spatial resolution than previous large-scale snow depth maps.~~ The performance of extensive and significant accuracy assessments has shown a high reliability of the processed winter-DSM based on the Vexcel Ultracam Eagle M3 sensor with an accuracy of approximately ~~0.1 to~~ 0. 15 m (Fig. 10). The accuracy assessment of the reference ALS-DTM compared to reference points (RMSE 0.03 m) has also demonstrated its high reliability. Therefore, the accuracy achieved in the winter-DSMs corresponds approximately to the actual accuracy of the calculated snow depth values. These accuracies of the snow depths match with the best results in Eberhard et al. (2021) and ~~-~~Meyer et al. (2022) ~~and fulfil the requirement of exact accurate snow depth mapping.~~

The strength of the presented ~~robustness of the~~ workflow ~~used in this study~~ is the robustness that is demonstrated through the quality grades of the snow depth maps despite difficult and complex acquisition conditions in high-mountain regions~~Accordingly, despite the difficult and varying acquisition conditions, which often occuroccurring in high mountain regions, the quality grades of the snow depth maps demonstrate the robustness of the workflow used in this study~~. In addition, excellent acquisition conditions such as in the year 2020 resulted in no significant improvements of the quality metrics.

A crucial disadvantage of ~~this~~ our workflow compared to the one of ~~–~~ Meyer et al. (2022) ~~Meyer et al. (2021)~~ is the necessity of 2 to 5 GCPs. Little effort was needed to measure the GCPs in the present study area due to the vicinity to the settlement, but this might be a limitation elsewhere~~sIn the presenting study area, the effort to measure the GCPs was low due to the vicinity to the WSL Institute for Snow and Avalanche Research SLF (SLF) Davos~~. T~~o capture remote regions, the exact processing of Ultracam data without GCPs would be necessary. A promising approach could be the~~his ~~might~~could be solved by using~~e~~ ~~of~~ a global coordinate system, but first experiences have shown~~,~~ that the accuracy is ~~considerably~~ lower and less reliable compared to our workflow. Under consideration of this limitation, the procedure is applicable on different study areas. Compared to the more expensive ALS-derived snow depth maps (Bühler et al. 2015; Deems et al. 2013; Painter et al. 2016) our computed metrics demonstrate an equal accuracy.

~~All computed metrics demonstrate an equal~~comparable ~~accuracy of our snow depth mapping compared to the one of an~~ose ~~derived from ALS (Painter et al. 2016; Deems et al. 2013), which would be connected to considerably higher costs (Bühler et al. 2015).~~ However, in areas with high vegetation or dense forests it is currently not possible to derive snow depths through photogrammetry~~The crucial disadvantages of this our photogrammetric method are still the problems in high vegetated and especially heavily forested areas~~. ~~Currently, there are d~~Different approaches have been proposed to ~~capture~~obtain ~~the~~ snow depth with photogrammetric methods within forested areas (i.e. (Broxton und van Leeuwen 2020; Harder et al. 2020), ~~but~~ yet the ~~dense forests in~~ steep slopes in combination with dense forests around Davos impeded the ~~the accurate and reliable recording of these areas~~processing ~~yet~~.

To counteract wrong values in those problematic areas, ~~different masks were used to increase the reliability of the snow depths.~~

~~This unique A~~a similar masking approach to ours was previously applied in Bühler et al. (2015), but the algorithm we used ~~in our study~~ has been~~is~~ considerably improved and is more reliable. ~~Another important characteristic of these masks is the almost automatic and consistent processing. Only the selection of streets and striking rivers requires manual interaction. In general, th~~The~~e~~ masks that we processed consistently and reproducible~~almost automatically~~, are characteris~~z~~ed by a high accuracy, but also exhibit little~~few~~ errors and limitations. In total, the percentage of incorrectly masked areas amounts to less than 1 %, which is considered satisfactory. ~~for the accurate and consistent~~automatic processing. The errors include for example snow-covered pixels in heavily shaded areas and snow mixed with soil falsely classified as no snow. Additional errors encompass new buildings, ignored single trees or environmental changes caused by mass movements. ~~The errors include snow covered pixels in heavily shaded areas or snow mixed with soil falsely classified as no snow as well as not considered single trees, newly built buildings or environmental changes through mass movements.~~ As those changes are inevitable in ~~the existing~~

~~structure of~~ our study and the values only account for a small proportion of our masks, we assess their effects as negligible. The transferability of the masks to other study areas depends on the data availability of existing forests and settlements. ~~As for transferability to other study areas, the implementation of the masks depends on the availability of~~ data for the extent of the ~~existing forests and settlements~~ an exactly classified ALS data of the snow-free terrain. ~~This is a crucial limitation of the method we used and would need adaption and evaluation of masks derived by other data sources.~~

6.2 Applications

The remarkable characteristics of the snow depth maps and the corresponding orthophotos enable new possibilities for various applications in science and practice~~.~~: T~~In particular, t~~he assessment and prevention of natural hazards, research on snow depth distribution processes and snow-hydrological models as well as other measurement methods. ~~can benefit from this unique data and the method used.~~ In the following sections we would like to discuss the relevance and potential impact of our work on selected applications.

~~6.1.1~~6.2.1 Natural hazards

The investigation of natural hazards such as snow avalanches or snow loadings on buildings can benefit from the presented snow depth maps and the approach applied. Studies of Bühler et al. (2019), Hafner et al. (2021), Eckerstorfer et al. (2019) and Leinss et al. (2020) have already demonstrated the importance and ~~the~~ limitations of manual as well as automatic large-scale avalanche mapping with satellite data. On a smaller scale Korzeniowska et al. (2017) proved the automatic detection of avalanches on the basis of orthophotos derived from airborne photogrammetry (sensor ADS80). Due to better radiometric characterisations and better spatial resolution of our orthophotos, even more details could be obtained than in previous studies. Furthermore, different studies (Peitzsch et al. 2015) have already suggested that the locations of glide-snow avalanches ~~is~~ are often similar between winters. Our data series ~~The location of the avalanches in our snow depth maps between the years show, that they are characterisz~~ed ~~through a high conformity. Correspondingly, these observations can reinforce previously~~confirms this finding ~~findings of the location of avalanches~~.

As exemplary shown in Fig. 13, the high-resolution orthophoto ~~would~~ allows for the exact identification of snow avalanches and associated release ~~zones~~ and deposition zones over larger regions. In numerous cases, the detection of the fracture line of an avalanche is possible as well. Consequently, the snow depth distribution around the avalanche fracture line ~~of the avalanche~~ can provide meaningful information about the release height and ~~therefore the release~~ volume.

However, release zones covered by new or wind-drifted snow, or avalanches released in extremely steep and complex terrain can be~~lead to~~ difficult to identif~~ication~~y ~~or inaccuracies of the release height~~. ~~Deviations of the snow height exceeding 0.3 m are unsuitable for the correct assessment of release zones.~~ Nevertheless, these snow depth maps are the first study ~~data, which~~to enable the determination of release heights of distinctive avalanches within larger regions. ~~The examination of release~~

heights with remote sensing methods is only sparsely explored. OSince so far only individual studies with UAS were able to accurately identify the release height so far (Souckova und Juras 2020; Proksch et al. 2018; Bühler et al. 2017), . , this is a considerable improvement. Furthermore, the assessment of snow volumes in release and deposition zones on the basis of snow depth maps and orthophotos facilitate the research on avalanche activities and characteristics of the corresponding periods. Studies with UAS have already demonstrated the high importance of these measurements (Bühler et al. 2017; Eckerstorfer et al. 2016).

The crucial advantage of our procedure compared to previously performed studies with the UASs is the ability to cover of larger areas during periods with high avalanche activity. However, the necessity of the flight permission and the weather-dependence often prevents short-term missions.

The assessment of other hazards such as snow loading on buildings or flooding caused by rapid snow melting can also be assisted by large-scale snow depth maps. For the determination of snow loadsing on buildings, an adaption of our workflow would be required by using the DSM of the ALS as a reference dataset and notrefraining from masking out settled areasments. Therefore, our accurate snow depth mapping facilitates the assessment of dangerous snow loading on roofs.

6.2.2 Planning and evaluation of avalanche protection structures protective constructions and automatic weather stations

Avalanche fences and other avalanche protection structures are crucial in alpine regions for the protection of infrastructure and residents. Protective constructions such as avalanche fences, have a crucial meaningare crucial for the civil protection in alpine regions. However, the functionality of avalanche fences is only guaranteed if they are correctly placed and have a sufficient heightHowever, the functionality of avalanche fences is only ensured guaranteed if they are placed in the ideal place location and if they exhibit a sufficient height (Margreth 2007). In our case, the snow depth map in 2019 demonstrates that the investigated wind-drift snow fences are too closely located to the release zone (Figure 14). This , and increasesinged the snow accumulation within the release zonesthese areas (Bühler et al. 2018a) and reducescinged the protectiveion effect. Since large parts of the fences were buried by snow in 2019, the existing current height and location of these fences could may not be not sufficient to prevent avalanche releases during critical avalanche periods. Accordingly, the snow depth maps can be used as for large-scale evaluation of existing as well as planned of existing avalanche protection constructionsstructures as well as the planning of . The information about the snow depth distribution also serves as basis for a successful planning of future avalancheadditional constructions protection structures (Prokop und Procter 2016). Switzerland has acknowledged the importance of snow distribution for the planning of new protection infrastructure and has included it in and . Ttherefore, snow depth maps derived from UAS, or airplane photogrammetry are established within are established in the construction processplanning process in Switzerland.

Furthermore, the suitabilitysnow depth representativity map (Figure 16) demonstrates how our snow depth maps can be implementedused in existing models to evaluate existing AWS sites and facilitates the location identification finding of suitable location for new AWSs which play a key role for different forecasts such as for the avalanche warning service (Pérez-

Guillén et al. 2022). Our snow depth mapsresults presented led to the assessment of a suitable location with a high representativity construction of the a new AWS atfor the new AWSLu Lukschalp- (in the Dischma vVvalley) which was built induring the summer of 2022. The snow depth values originate here from our large-scale snow depth maps Similar snow depth maps as well as the gained knowledge about snow depth distribution pattern will be applied for the planning of new AWS. and similar approached will be applied for further planning of new AWS.

In addition, our snow depth maps enable the assessment of the representativity of existing long-term AWS around Davos, which were are used for various projects and the avalanche forecasting. Previously, the representativity of these stations was qualitatively assessed by experts, but now, our snow depth maps allow enable the comparison of spatial snow depth measurements in open areas with the station measurements (-)with these values. However, the presented results only represent the peak of winter date, accordingly, during early winter or melt season, the relation between point snow measurements to spatial snow dept distribution could be different due to changing energy balances. Further investigations are required to confirm similar snow depth distribution pattern over the entire winter season and to enable accurate interpolations from point measurement (AWS) to entire catchments.

6.1.26.2.3 Analysis of specific Ssnow depth distribution features

Our snow depth maps play a key role in better understanding the snow depth distribution in alpine terrainOur snow depth maps could be a key for the better understanding of snow depth distribution in alpine terrain, which influences numerous sectors. The results presented in Fig. 11 and Table 6 show the strongly varying average snow depths. , which corresponds to the observations of the snow depth maps by Marty et al. (2019) and point out the added value of annual snow depth maps (Marty et al. 2019). Despite the high difference of the average snow depths, we identified a similar relative snow depth distribution, which was exemplary shown in the normalized snow depth maps in (Fig. 12). Consequently, the relative snow depth distribution between different years is almost independent of the average snow depths with the exception of separate avalanche depositions zones and selected special features as they do not occur every year.

Since different publications had already described different snow depth distribution patterns, they will be discussed on the basis of our results. The studies of – Grünewald et al. (2014) and Prokop (2008) found, that snow at wind-exposed and steep areas is relocated to flatter areas and sinks. Our results confirm these observations. For example, small creeks in high-mountain catchments can be identified on the snow depth distribution in our snow depth maps, because the creeks are filled up with snow and exactly these pixels exhibit higher snow depths than surrounding areas. Similar features can be recognised in drainage channels in extremely steep slopes.

Bühler et al. (2015) and Schirmer et al. (2011) recogniszed the permanent occurrencere-occurrence of cornices at the same ridges around the Wannengrat within our study area in two different years. Our data can verify the formation of this cornice in further subsequent years. In addition, we determine the re-occurrence of cornices at the same locations in all of our assessed yearsIn addition, we determine the persistent formation of cornices in all years of the time series at numerous ridges. These cornices lead to considerably higher snow depths on the same side in each winter. Furthermore, different studies (Peitzsch et

al. 2015). have already suggested that the location of glide-snow avalanches is often similar between winters. The location of the avalanches in our snow depth maps between the years show, that they are characterized through a high conformity. Correspondingly, these observations can reinforce previously findings of the location of avalanches.

These Our observations concerning the relative snow distribution correspond to the results of Schirmer et al. (2011) and Wirz et al. (2011), which already found higher and lower relative snow depths on the same locations within a winter, respectively. However, all these studies were either temporally limited to only one year (Schirmer et al. 2011; Wirz et al. 2011) or the accuracy and the spatial resolution of the snow depth maps (Bühler et al. 2015; Marty et al. 2019) complicated the investigation of snow depth distribution patterns. Therefore, our snow depth maps as are the first time-series which enables the an extensive large-scale comparison of snow depth distribution between different years on a large scale. These new possibilities lead to the confirmation of different theoretical approaches, which assumed that the snow depth distribution is more dependent on terrain characteristics than on the weather conditions of a certain year. This revelation opens new possibilities for the modelling of snow depths over large regions.

6.1.36.2.4 Validation dataset

Different studies have already benefited from the existing unique time-series of large snow depth maps (ADS sensor) processed by Marty et al. (2019). However, the inaccuracies and the lower reliability of these snow depth maps also limited the validation and evaluation of other studies. In particular, deepDeep learning approaches or studies which are calibrated by exact reference data can now benefit from our improved quality. Therefore, it is to be to be expected, that the our data and approach will be applied used in numerous studies. For example, the snow depth maps serve as training dataset for a running project to improve the modelling of the daily snow depth distribution in Switzerland. Without our data, the model was not able to represent the snow depth distribution in complex terrain. In addition, our data could correct modelled snow depth maps which for example often exhibit a bias towards an overassessment of snow depths in high-mountain region.

In addition, Oour data could also validate or evaluate numerous projects in conjunction with hydrological and snow modellings (Helbig et al. 2021; Richter et al. 2021; Vögeli et al. 2016), wind-drift models (Gerber et al. 2017; Mott et al. 2010; Schön et al. 2015), automatic detection of avalanche release zones (Bühler et al. 2018b; Bühler et al. 2022) and further snow depth models or snow depth measurements on the basis of satellite data (Leiterer et al. 2020; Wulf et al. 2020).

7 Conclusions

In this study we present the development, validation and application of a consistent and robust workflow to process aerial imagery from the state-of-the-art survey camera Vexcel Ultracam to produce reliable snow depth maps. We demonstrate its capability to capture large areas covering more than 100 km² under optimal as well as suboptimal acquisition conditions (varying illumination, clouds, new snow cover, the absence of the NIR-band). The accuracies of our snow depth maps (RMSE:

0.15 m, Ultracam Eagle M3) are similar to results achieved with ALS and fulfil the requirements for meaningful, spatially continuous snow depth mapping in ~~complex~~ complex, open terrain. The metrics are calculated by applying an extensive accuracy assessment with check points, comparisons to UAS-derived DSMs and the evaluations of snow-free pixels, revealing a very high quality even within steep terrain. The reliability of our maps allows for the comparison of ~~the~~ snow depth values within a 5-year period, which have shown that despite large differences of the average snow depth, the relative snow depth distribution and the formation of small-scale features is similar throughout the years.

Restrictions of the data and its acquisition are the relatively high data acquisition costs (approximately ~~US$~~ 20'000 CHF for 300 km^2) and the availability of a piloted aircraft and corresponding permissions. In addition, the ~~developed~~ procedure is limited by widespread low clouds, areas with high vegetation such as forests ~~and bushes~~, the availability of accurate snow-free DTMs and powerful hardware ~~with large storage for processing~~. ~~Even though~~Even though accurate GNSS and IMU data is available from the airplane, one to five ground control points (GCPs, distribution is not important) as well as the ~~almost automatically~~consistent calculated masks are essential to achieve reliable results.

In particular, the high spatial resolution of our maps (0.5 m) and orthophotos (0.25 m) in ~~connection~~ conjunction with the achieved accuracy, offer the possibility to better understand the complexity of snow depth distribution in high-mountain regions. Based on the presented products, models of water stored in the snowpack (SWE) can be evaluated and improved, ~~this~~ which is for example crucial for hydropower generation. New approaches to map snow depth with optical and radar satellites from space can be evaluated. Also, the investigation of snow avalanches benefits from such data. Several running research projects are already applying our maps for validation. We expect that in the coming years, our data will ~~become a key~~play a key role ~~for~~ in numerous new findings in snow science ~~in the coming years~~.

The improvement of photogrammetry within ~~areas covered by~~ alpine forests would be a significant step forward to equalize with the advantages of ALS. ~~Our data has already been used to validate and evaluate different research projects.~~ Our data allows for the extrapolation of the snow depth distribution from small areas, mapped for example by UAS, to the scale of large catchments. To further enhance the value of photogrammetric snow depth mapping, the current time series will be extended into the future. Together with datasets acquired from 2010 to 2016 with the ADS sensor within the same region, we established a~~n~~ unique eleven-year snow depth time series.

Data availability. The datasets used in this study will be published in ENVIDAT (https://www.envidat.ch) with the final publication of this study.

Author contributions. YB and LB designed the study. YB, AS, EH and LAE performed the fieldwork. LB processed the data with inputs from MM and YB. LB and YB prepared the manuscript with contributions from all co-authors.

Competing interests. The authors declare that they have no conflict of interest.

Acknowledgements. We would like to thank the Swiss National Science Foundation (SNF; Grant N° 200021_172800) for partly funding this project. We also thank the assistants for their help during the various fieldworks.

Financial support. This research has been partially supported by the Swiss National Science Foundation (SNF; Grant N° 200021_172800).

8 Literaturverzeichnis

Adams, Marc S.; Bühler, Yves; Fromm, Reinhard (2018): Multitemporal Accuracy and Precision Assessment of Unmanned Aerial System Photogrammetry for Slope-Scale Snow Depth Maps in Alpine Terrain. In: *Pure Appl. Geophys.* 175 (9), S. 3303–3324. DOI: 10.1007/s00024-017-1748-y.

Agisoft LLC (2020): Agisoft Metashape User Manual. Professional Edition, Version 1.6. St. Petersburg.

Avanzi, Francesco; Bianchi, Alberto; Cina, Alberto; Michele, Carlo de; Maschio, Paolo; Pagliari, Diana et al. (2018): Centimetric Accuracy in Snow Depth Using Unmanned Aerial System Photogrammetry and a MultiStation. In: *Remote Sensing* 10 (5), S. 765. DOI: 10.3390/rs10050765.

Brauchli, Tristan; Trujillo, Ernesto; Huwald, Hendrik; Lehning, Michael (2017): Influence of Slope-Scale Snowmelt on Catchment Response Simulated With the Alpine3D Model. In: *Water Resour. Res.* 53 (12), S. 10723–10739. DOI: 10.1002/2017WR021278.

Broxton, Patrick D.; van Leeuwen, Willem J. D. (2020): Structure from Motion of Multi-Angle RPAS Imagery Complements Larger-Scale Airborne Lidar Data for Cost-Effective Snow Monitoring in Mountain Forests. In: *Remote Sensing* 12 (14), S. 2311. DOI: 10.3390/rs12142311.

Brun, E.; David, P.; Sudul, M.; Brunot, G. (1992): A numerical model to simulate snow-cover stratigraphy for operational avalanche forecasting. In: *J. Glaciol.* 38 (128), S. 13–22. DOI: 10.3189/S0022143000009552.

Bühler, Y.; Bührle, L.; Eberhard, L.; Marty, M.; & Stoffel, A. (2021): Grossflächige Schneehöhen-Kartierung mit Flugzeug und Satellit. In: *Geomatik Schweiz* (119), Artikel 212 - 215.

Bühler, Y.; Eberhard, L.; Feuerstein, G.; Lurati, D.; Guler, A.; Margreth, S. (2018a): Drohneneinsatz für die Kartierung der Schneehöhenverteilung. In: *Bündnerwald* (71), S. 20–25.

Bühler, Y.; Marty, M.; Egli, L.; Veitinger, J.; Jonas, T.; Thee, P.; Ginzler, C. (2015): Snow depth mapping in high-alpine catchments using digital photogrammetry. In: *The Cryosphere* 9 (1), S. 229–243. DOI: 10.5194/tc-9-229-2015.

Bühler, Yves; Adams, Marc S.; Bösch, Ruedi; Stoffel, Andreas (2016): Mapping snow depth in alpine terrain with unmanned aerial systems (UASs): potential and limitations. In: *The Cryosphere* 10 (3), S. 1075–1088. DOI: 10.5194/tc-10-1075-2016.

Bühler, Yves; Adams, Marc S.; Stoffel, Andreas; Boesch, Ruedi (2017): Photogrammetric reconstruction of homogenous snow surfaces in alpine terrain applying near-infrared UAS imagery. In: *International Journal of Remote Sensing* 38 (8-10), S. 3135–3158. DOI: 10.1080/01431161.2016.1275060.

Bühler, Yves; Bebi, Peter; Christen, Marc; Margreth, Stefan; Stoffel, Lukas; Stoffel, Andreas et al. (2022): Automated avalanche hazard indication mapping on state wide scale.

Bühler, Yves; Hafner, Elisabeth D.; Zweifel, Benjamin; Zesiger, Mathias; Heisig, Holger (2019): Where are the avalanches? Rapid SPOT6 satellite data acquisition to map an extreme avalanche period over the Swiss Alps. In: *The Cryosphere* 13 (12), S. 3225–3238. DOI: 10.5194/tc-13-3225-2019.

Bühler, Yves; Rickenbach, Daniel von; Stoffel, Andreas; Margreth, Stefan; Stoffel, Lukas; Christen, Marc (2018b): Automated snow avalanche release area delineation – validation of existing algorithms and proposition of a new object-based approach for large-scale hazard indication mapping. In: *Nat. Hazards Earth Syst. Sci.* 18 (12), S. 3235–3251. DOI: 10.5194/nhess-18-3235-2018.

Bührle, Leon (2021): Creation, accuracy assessment and comparison of snow depth maps around Davos from Ultracam data from 2017 to 2021. Innsbruck.

Christen, M.; Kowalski, J.; Bartelt, P. (2010): RAMMS: Numerical simulation of dense snow avalanches in three-dimensional terrain. In: *Cold Regions Science and Technology* 63 (1-2), S. 1–14. DOI: 10.1016/j.coldregions.2010.04.005.

Croce, Pietro; Formichi, Paolo; Landi, Filippo; Mercogliano, Paola; Bucchignani, Edoardo; Dosio, Alessandro; Dimova, Silvia (2018): The snow load in Europe and the climate change. In: *Climate Risk Management* 20, S. 138–154. DOI: 10.1016/j.crm.2018.03.001.

Deems, Jeffrey S.; Painter, Thomas H.; Finnegan, David C. (2013): Lidar measurement of snow depth: a review. In: *J. Glaciol.* 59 (215), S. 467–479. DOI: 10.3189/2013JoG12J154.

Deschamps-Berger, César; Gascoin, Simon; Berthier, Etienne; Deems, Jeffrey; Gutmann, Ethan; Dehecq, Amaury et al. (2020): Snow depth mapping from stereo satellite imagery in mountainous terrain: evaluation using airborne laser-scanning data. In: *The Cryosphere* 14 (9), S. 2925–2940. DOI: 10.5194/tc-14-2925-2020.

Dozier, Jeff (1989): Spectral signature of alpine snow cover from the landsat thematic mapper. In: *Remote Sensing of Environment* 28, S. 9–22. DOI: 10.1016/0034-4257(89)90101-6.

Eberhard, Lucie A.; Sirguey, Pascal; Miller, Aubrey; Marty, Mauro; Schindler, Konrad; Stoffel, Andreas; Bühler, Yves (2021): Intercomparison of photogrammetric platforms for spatially continuous snow depth mapping. In: *The Cryosphere* 15 (1), S. 69–94. DOI: 10.5194/tc-15-69-2021.

Eckerstorfer, Markus; Bühler, Yves; Frauenfelder, Regula; Malnes, Eirik (2016): Remote sensing of snow avalanches: Recent advances, potential, and limitations. In: *Cold Regions Science and Technology* 121, S. 126–140. DOI: 10.1016/j.coldregions.2015.11.001.

Eckerstorfer, Markus; Vickers, Hannah; Malnes, Eirik; Grahn, Jakob (2019): Near-Real Time Automatic Snow Avalanche Activity Monitoring System Using Sentinel-1 SAR Data in Norway. In: *Remote Sensing* 11 (23), S. 2863. DOI: 10.3390/rs11232863.

Eker, Remzi; Bühler, Yves; Schlögl, Sebastian; Stoffel, Andreas; Aydın, Abdurrahim (2019): Monitoring of Snow Cover Ablation Using Very High Spatial Resolution Remote Sensing Datasets. In: *Remote Sensing* 11 (6), S. 699. DOI: 10.3390/rs11060699.

Essery, R. (2015): A factorial snowpack model (FSM 1.0). In: *Geosci. Model Dev.* 8 (12), S. 3867–3876. DOI: 10.5194/gmd-8-3867-2015.

Federal Office of Topography swisstopo (2021a): LiDAR data acquisition. Online verfügbar unter https://www.swisstopo.admin.ch/en/knowledge-facts/geoinformation/lidar-data.html, zuletzt geprüft am 02.11.2021.

Federal Office of Topography swisstopo (2021b): REFRAME. Online verfügbar unter https://www.swisstopo.admin.ch/en/maps-data-online/calculation-services/reframe.html, zuletzt geprüft am 02.11.2021.

Federal Office of Topography swisstopo (2021c): swissTLM3D. Online verfügbar unter https://www.swisstopo.admin.ch/en/geodata/landscape/tlm3d.html, zuletzt geprüft am 03.11.2021.

Feistl, T.; Bebi, P.; Dreier, L.; Hanewinkel, M.; Bartelt, P. (2014): Quantification of basal friction for technical and silvicultural glide-snow avalanche mitigation measures. In: *Nat. Hazards Earth Syst. Sci.* 14 (11), S. 2921–2931. DOI: 10.5194/nhess-14-2921-2014.

Gerber, F.; Lehning, M.; Hoch, S. W.; Mott, R. (2017): A close-ridge small-scale atmospheric flow field and its influence on snow accumulation. In: *J. Geophys. Res. Atmos.* 122 (15), S. 7737–7754. DOI: 10.1002/2016JD026258.

Gerber, Franziska; Mott, Rebecca; Lehning, Michael (2019): The Importance of Near-Surface Winter Precipitation Processes in Complex Alpine Terrain. In: *Journal of Hydrometeorology* 20 (2), S. 177–196. DOI: 10.1175/JHM-D-18-0055.1.

Gindraux, Saskia; Boesch, Ruedi; Farinotti, Daniel (2017): Accuracy Assessment of Digital Surface Models from Unmanned Aerial Vehicles' Imagery on Glaciers. In: *Remote Sensing* 9 (2), S. 186. DOI: 10.3390/rs9020186.

GLAMOS - Glacier Monitoring Switzerland (2021): Swiss Glacier Mass Balance 2020 (release 2021). Unter Mitarbeit von Matthias Huss, Andreas Bauder, Mauro Fischer, Martin Funk, Giovanni Kappenberger, Andreas Linsbauer et al.

Griessinger, Nena; Mohr, Franziska; Jonas, Tobias (2018): Measuring snow ablation rates in alpine terrain with a mobile multioffset ground-penetrating radar system. In: *Hydrol. Process.* DOI: 10.1002/hyp.13259.

Grünewald, T.; Bühler, Y.; Lehning, M. (2014): Elevation dependency of mountain snow depth. In: *The Cryosphere* 8 (6), S. 2381–2394. DOI: 10.5194/tc-8-2381-2014.

Grünewald, T.; Schirmer, M.; Mott, R.; Lehning, M. (2010): Spatial and temporal variability of snow depth and ablation rates in a small mountain catchment. In: *The Cryosphere* 4 (2), S. 215–225. DOI: 10.5194/tc-4-215-2010.

Hafner, Elisabeth D.; Techel, Frank; Leinss, Silvan; Bühler, Yves (2021): Mapping avalanches with satellites – evaluation of performance and completeness. In: *The Cryosphere* 15 (2), S. 983–1004. DOI: 10.5194/tc-15-983-2021.

Hall, Dorothy K.; Riggs, George A.; Salomonson, Vincent V. (1995): Development of methods for mapping global snow cover using moderate resolution imaging spectroradiometer data. In: *Remote Sensing of Environment* 54 (2), S. 127–140. DOI: 10.1016/0034-4257(95)00137-P.

Harder, Phillip; Pomeroy, John W.; Helgason, Warren D. (2020): Improving sub-canopy snow depth mapping with unmanned aerial vehicles: lidar versus structure-from-motion techniques. In: *The Cryosphere* 14 (6), S. 1919–1935. DOI: 10.5194/tc-14-1919-2020.

Harder, Phillip; Schirmer, Michael; Pomeroy, John; Helgason, Warren (2016): Accuracy of snow depth estimation in mountain and prairie environments by an unmanned aerial vehicle. In: *The Cryosphere* 10 (6), S. 2559–2571. DOI: 10.5194/tc-10-2559-2016.

Helbig, Nora; Bühler, Yves; Eberhard, Lucie; Deschamps-Berger, César; Gascoin, Simon; Dumont, Marie et al. (2021): Fractional snow-covered area: scale-independent peak of winter parameterization. In: *The Cryosphere* 15 (2), S. 615–632. DOI: 10.5194/tc-15-615-2021.

Helfricht, K.; Kuhn, M.; Keuschnig, M.; Heilig, A. (2014): Lidar snow cover studies on glaciers in the Ötztal Alps (Austria): comparison with snow depths calculated from GPR measurements. In: *The Cryosphere* 8 (1), S. 41–57. DOI: 10.5194/tc-8-41-2014.

Höhle, Joachim; Höhle, Michael (2009): Accuracy assessment of digital elevation models by means of robust statistical methods. In: *ISPRS Journal of Photogrammetry and Remote Sensing* 64 (4), S. 398–406. DOI: 10.1016/j.isprsjprs.2009.02.003.

Jacobs, Jennifer M.; Hunsaker, Adam G.; Sullivan, Franklin B.; Palace, Michael; Burakowski, Elizabeth A.; Herrick, Christina; Cho, Eunsang (2021): Snow depth mapping with unpiloted aerial system lidar observations: a case study in Durham, New Hampshire, United States. In: *The Cryosphere* 15 (3), S. 1485–1500. DOI: 10.5194/tc-15-1485-2021.

Koenderink, J. J.; van Doorn, A. J. (1991): Affine structure from motion. In: *Journal of the Optical Society of America. A, Optics and image science* 8 (2), S. 377–385. DOI: 10.1364/JOSAA.8.000377.

Korzeniowska, Karolina; Bühler, Yves; Marty, Mauro; Korup, Oliver (2017): Regional snow-avalanche detection using object-based image analysis of near-infrared aerial imagery. In: *Nat. Hazards Earth Syst. Sci.* 17 (10), S. 1823–1836. DOI: 10.5194/nhess-17-1823-2017.

Kulakowski, Dominik; Bebi, Peter; Rixen, Christian (2011): The interacting effects of land use change, climate change and suppression of natural disturbances on landscape forest structure in the Swiss Alps. In: *Oikos* 120 (2), S. 216–225. DOI: 10.1111/j.1600-0706.2010.18726.x.

Leinss, Silvan; Wicki, Raphael; Holenstein, Sämi; Baffelli, Simone; Bühler, Yves (2020): Snow avalanche detection and mapping in multitemporal and multiorbital radar images from TerraSAR-X and Sentinel-1. In: *Nat. Hazards Earth Syst. Sci.* 20 (6), S. 1783–1803. DOI: 10.5194/nhess-20-1783-2020.

Leiterer, Reik; Wulf, Hendri; Milani, Gillian; Sassik, Bernhard; Bühler, Yves; Wegner, Jan (2020): Schneekartierung aus dem All – das Potenzial frei verfügbarer Satellitendaten. In: *«Wasser Energie Luft* (3), S. 171–174.

Linsbauer, Andreas; Huss, Matthias; Hodel, Elias; Bauder, Andreas; Fischer, Mauro; Weidmann, Yvo et al. (2021): The New Swiss Glacier Inventory SGI2016: From a Topographical to a Glaciological Dataset. In: *Front. Earth Sci.* 9, Artikel 704189. DOI: 10.3389/feart.2021.704189.

López-Moreno, Juan I.; Revuelto, Jesús; Alonso-González, E.; Sanmiguel-Vallelado, Alba; Fassnacht, Steven R.; Deems, Jeffrey; Morán-Tejeda, Enrique (2017): Using very long-range terrestrial laser scanner to analyze the temporal consistency of the snowpack distribution in a high mountain environment. In: *J. Mt. Sci.* 14 (5), S. 823–842. DOI: 10.1007/s11629-016-4086-0.

Lowe, David G. (2004): Distinctive Image Features from Scale-Invariant Keypoints. In: *International Journal of Computer Vision* 60 (2), S. 91–110. DOI: 10.1023/B:VISI.0000029664.99615.94.

Magnusson, Jan; Nævdal, Geir; Matt, Felix; Burkhart, John F.; Winstral, Adam (2020): Improving hydropower inflow forecasts by assimilating snow data. In: *Hydrology Research* 51 (2), S. 226–237. DOI: 10.2166/nh.2020.025.

Margreth, Stefan (2007): Defense structures in avalanche starting zones. Technical guideline as an aid to enforcement.

Marti, R.; Gascoin, S.; Berthier, E.; Pinel, M. de; Houet, T.; Laffly, D. (2016): Mapping snow depth in open alpine terrain from stereo satellite imagery. In: *The Cryosphere* 10 (4), S. 1361–1380. DOI: 10.5194/tc-10-1361-2016.

Marty, M.; Bühler, Y.; Ginzler, C. (2019): Snow Depth Mapping. Unter Mitarbeit von Mauro Marty.

Mazzotti, Giulia; Currier, William Ryan; Deems, Jeffrey S.; Pflug, Justin M.; Lundquist, Jessica D.; Jonas, Tobias (2019): Revisiting Snow Cover Variability and Canopy Structure Within Forest Stands: Insights From Airborne Lidar Data. In: *Water Resour. Res.* 55 (7), S. 6198–6216. DOI: 10.1029/2019WR024898.

McGrath, Daniel; Webb, Ryan; Shean, David; Bonnell, Randall; Marshall, Hans-Peter; Painter, Thomas H. et al. (2019): Spatially Extensive Ground-Penetrating Radar Snow Depth Observations During NASA's 2017 SnowEx Campaign: Comparison With In Situ, Airborne, and Satellite Observations. In: *Water Resour. Res.* 55 (11), S. 10026–10036. DOI: 10.1029/2019WR024907.

Meyer, Joachim; Deems, Jeffrey S.; Bormann, Kat J.; Shean, David E.; Skiles, S. McKenzie (2022): Mapping snow depth and volume at the alpine watershed scale from aerial imagery using Structure from Motion. In: *Front. Earth Sci.* 10, Artikel 989792. DOI: 10.3389/feart.2022.989792.

Meyer, Joachim; Skiles, S. McKenzie (2019): Assessing the Ability of Structure From Motion to Map High-Resolution Snow Surface Elevations in Complex Terrain: A Case Study From Senator Beck Basin, CO. In: *Water Resour. Res.* 55 (8), S. 6596–6605. DOI: 10.1029/2018WR024518.

Michele, Carlo de; Avanzi, Francesco; Passoni, Daniele; Barzaghi, Riccardo; Pinto, Livio; Dosso, Paolo et al. (2016): Using a fixed-wing UAS to map snow depth distribution: an evaluation at peak accumulation. In: *The Cryosphere* 10 (2), S. 511–522. DOI: 10.5194/tc-10-511-2016.

Mietkiewicz, Nathan; Kulakowski, Dominik; Rogan, John; Bebi, Peter (2017): Long-term change in sub-alpine forest cover, tree line and species composition in the Swiss Alps. In: *J Veg Sci* 28 (5), S. 951–964. DOI: 10.1111/jvs.12561.

Miller, Zachary S.; Peitzsch, Erich H.; Sproles, Eric A.; Birkeland, Karl W.; Palomaki, Ross T. (2022): Assessing the seasonal evolution of snow depth spatial variability and scaling in complex mountain terrain. In: *The Cryosphere* 16 (12), S. 4907–4930. DOI: 10.5194/tc-16-4907-2022.

Mott, R.; Schirmer, M.; Bavay, M.; Grünewald, T.; Lehning, M. (2010): Understanding snow-transport processes shaping the mountain snow-cover. In: *The Cryosphere* 4 (4), S. 545–559. DOI: 10.5194/tc-4-545-2010.

Nolan, M.; Larsen, C.; Sturm, M. (2015): Mapping snow depth from manned aircraft on landscape scales at centimeter resolution using structure-from-motion photogrammetry. In: *The Cryosphere* 9 (4), S. 1445–1463. DOI: 10.5194/tc-9-1445-2015.

Painter, Thomas H.; Berisford, Daniel F.; Boardman, Joseph W.; Bormann, Kathryn J.; Deems, Jeffrey S.; Gehrke, Frank et al. (2016): The Airborne Snow Observatory: Fusion of scanning lidar, imaging spectrometer, and physically-based modeling for mapping snow water equivalent and snow albedo. In: *Remote Sensing of Environment* 184, S. 139–152. DOI: 10.1016/j.rse.2016.06.018.

Peitzsch, Erich H.; Hendrikx, Jordy; Fagre, Daniel B. (2015): Terrain parameters of glide snow avalanches and a simple spatial glide snow avalanche model. In: *Cold Regions Science and Technology* 120, S. 237–250. DOI: 10.1016/j.coldregions.2015.08.002.

Pérez-Guillén, Cristina; Techel, Frank; Hendrick, Martin; Volpi, Michele; van Herwijnen, Alec; Olevski, Tasko et al. (2022): Data-driven automated predictions of the avalanche danger level for dry-snow conditions in Switzerland. In: *Nat. Hazards Earth Syst. Sci.* 22 (6), S. 2031–2056. DOI: 10.5194/nhess-22-2031-2022.

Prokop, Alexander (2008): Assessing the applicability of terrestrial laser scanning for spatial snow depth measurements. In: *Cold Regions Science and Technology* 54 (3), S. 155–163. DOI: 10.1016/j.coldregions.2008.07.002.

Prokop, Alexander; Procter, Emily S. (2016): A new methodology for planning snow drift fences in alpine terrain. In: *Cold Regions Science and Technology* 132, S. 33–43. DOI: 10.1016/j.coldregions.2016.09.010.

Proksch, Martin; Dräyer, Bernhard; Pašić, Ivan; Burkard, André; Carlen, Norbert (2018): The valalanche project: Putting recent progress in snow avalanche mapping into practice. In: *International Snow Science Workshop*, S. 826–829.

Revuelto, Jesús; Alonso-Gonzalez, Esteban; Vidaller-Gayan, Ixeia; Lacroix, Emilien; Izagirre, Eñaut; Rodríguez-López, Guillermo; López-Moreno, Juan Ignacio (2021): Intercomparison of UAV platforms for mapping snow depth distribution in complex alpine terrain. In: *Cold Regions Science and Technology* 190, S. 103344. DOI: 10.1016/j.coldregions.2021.103344.

Richter, Bettina; Schweizer, Jürg; Rotach, Mathias W.; van Herwijnen, Alec (2021): Modeling spatially distributed snow instability at a regional scale using Alpine3D. In: *J. Glaciol.*, S. 1–16. DOI: 10.1017/jog.2021.61.

Rixen, Christian; Dawes, Melissa A.; Wipf, Sonja; Hagedorn, Frank (2012): Evidence of enhanced freezing damage in treeline plants during six years of CO2 enrichment and soil warming. In: *Oikos* 121 (10), S. 1532–1543. DOI: 10.1111/j.1600-0706.2011.20031.x.

Sanz-Ablanedo, Enoc; Chandler, Jim; Rodríguez-Pérez, José; Ordóñez, Celestino (2018): Accuracy of Unmanned Aerial Vehicle (UAV) and SfM Photogrammetry Survey as a Function of the Number and Location of Ground Control Points Used. In: *Remote Sensing* 10 (10), S. 1606. DOI: 10.3390/rs10101606.

Schirmer, M.; Wirz, V.; Clifton, A.; Lehning, M. (2011): Persistence in intra-annual snow depth distribution: 1. Measurements and topographic control. In: *Water Resour. Res.* 47 (9). DOI: 10.1029/2010WR009426.

Schlögl, Sebastian; Lehning, Michael; Fierz, Charles; Mott, Rebecca (2018): Representation of Horizontal Transport Processes in Snowmelt Modeling by Applying a Footprint Approach. In: *Front. Earth Sci.* 6, Artikel 120. DOI: 10.3389/feart.2018.00120.

Schneider, S.; Gruber, M. (2008): RADIOMETRIC QUALITY OF ULTRACAM-X IMAGES. In: *The International Archives of the Photogrammetry, Remote Sensing and Spatial Information Sciences* (37), S. 539–544.

Schön, Peter; Prokop, Alexander; Vionnet, Vincent; Guyomarc'h, Gilbert; Naaim-Bouvet, Florence; Heiser, Micha (2015): Improving a terrain-based parameter for the assessment of snow depths with TLS data in the Col du Lac Blanc area. In: *Cold Regions Science and Technology* 114, S. 15–26. DOI: 10.1016/j.coldregions.2015.02.005.

Shaw, Thomas E.; Gascoin, Simon; Mendoza, Pablo A.; Pellicciotti, Francesca; McPhee, James (2020): Snow Depth Patterns in a High Mountain Andean Catchment from Satellite Optical Tristereoscopic Remote Sensing. In: *Water Resour. Res.* 56 (2). DOI: 10.1029/2019WR024880.

Souckova, Marketa; Juras, Roman (2020): Mapping snow avalanche releases by unmanned aerial vehicles (UAV) in Krkonoše mountain range, the Czech Republic.

Spandre, Pierre; François, Hugues; Thibert, Emmanuel; Morin, Samuel; George-Marcelpoil, Emmanuelle (2017): Determination of snowmaking efficiency on a ski slope from observations and modelling of snowmaking events and seasonal snow accumulation. In: *The Cryosphere* 11 (2), S. 891–909. DOI: 10.5194/tc-11-891-2017.

Triggs, Bill; McLauchlan, Philip F.; Hartley, Richard I.; Fitzgibbon, Andrew W. (2000): Bundle Adjustment — A Modern Synthesis. In: Gerhard Goos, Juris Hartmanis, Jan van Leeuwen, Bill Triggs, Andrew Zisserman und Richard Szeliski (Hg.): Vision Algorithms: Theory and Practice, Bd. 1883. Berlin, Heidelberg: Springer Berlin Heidelberg (Lecture Notes in Computer Science), S. 298–372.

Vögeli, Christian; Lehning, Michael; Wever, Nander; Bavay, Mathias (2016): Scaling Precipitation Input to Spatially Distributed Hydrological Models by Measured Snow Distribution. In: *Front. Earth Sci.* 4. DOI: 10.3389/feart.2016.00108.

Westoby, M. J.; Brasington, J.; Glasser, N. F.; Hambrey, M. J.; Reynolds, J. M. (2012): 'Structure-from-Motion' photogrammetry: A low-cost, effective tool for geoscience applications. In: *Geomorphology* 179, S. 300–314. DOI: 10.1016/j.geomorph.2012.08.021.

Wipf, Sonja; Stoeckli, Veronika; Bebi, Peter (2009): Winter climate change in alpine tundra: plant responses to changes in snow depth and snowmelt timing. In: *Climatic Change* 94 (1-2), S. 105–121. DOI: 10.1007/s10584-009-9546-x.

Wirz, V.; Schirmer, M.; Gruber, S.; Lehning, M. (2011): Spatio-temporal measurements and analysis of snow depth in a rock face. In: *The Cryosphere* 5 (4), S. 893–905. DOI: 10.5194/tc-5-893-2011.

Wulf, Hendrik; Sassik, Bernhard; Milani, Gillian; Leiterer, Reik (2020): High-resolution snow depth monitoring for entire mountain ranges. In: 2020 7th Swiss Conference on Data Science (SDS). 2020 7th Swiss Conference on Data Science (SDS). Luzern, Switzerland, 26.06.2020 - 26.06.2020: IEEE, S. 1–4.

9 Appendix

Appendix A. Overview reference points in 2020

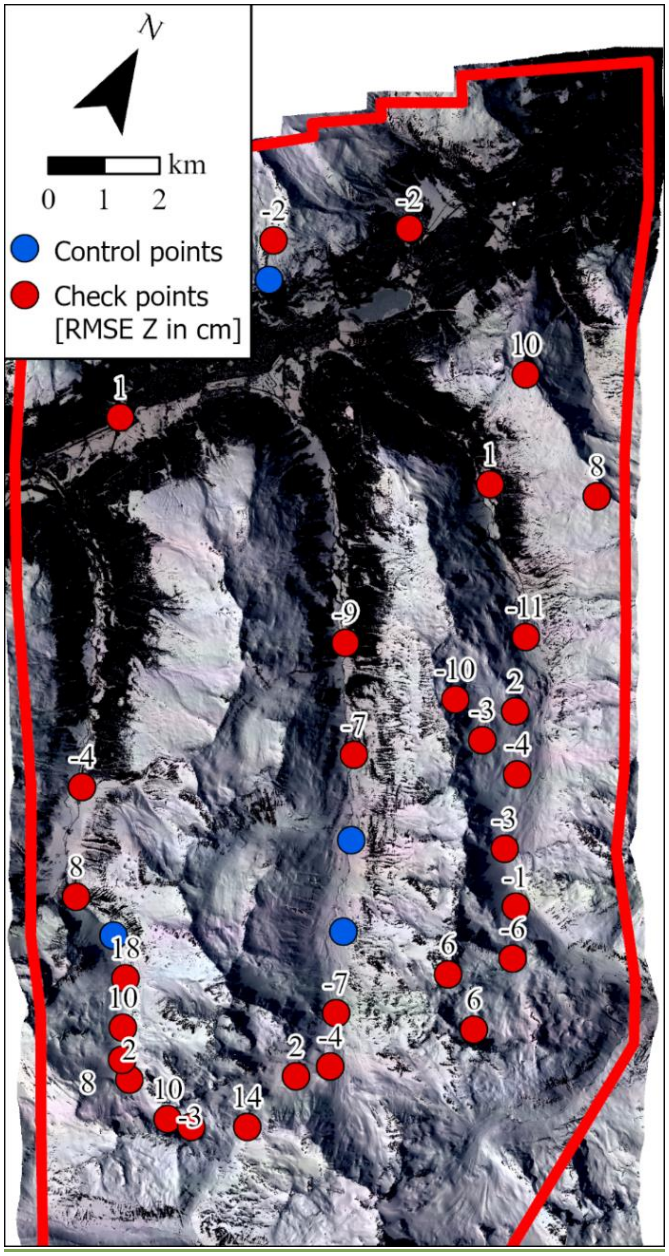

Figure A1. Overview of the distribution of ground control points (red) and check points (blue) with the corresponding RMSE Z values. Background shows the orthophoto from 2020.

Appendix ~~A~~B. Overview area and percentage of masks used.

~~Area [km²] and percentage [%] of various masks, outliers and remaining snow depth values for all snow depth maps~~

Table A2. Area [km²] and percentage [%] of various masks, outliers and remaining snow depth values for all snow depth maps.

Year		Waters	Glacier	Building & infrastructure	High vegetation	Outlier	Snow depth values
2017	Area [km²]	2.2	3.4	13.3	221.3	19.2	369.8
	Percentage [%]	0.3	0.5	2.1	35.2	3.0	58.8
2018	Area [km²]	0.3	0.0	4.5	30.7	0.2	35.6
	Percentage [%]	0.5	0.0	6.2	43.1	0.3	50.1
2019	Area [km²]	1.1	2.7	6.7	61.8	1.1	167.4
	Percentage [%]	0.5	1.1	2.7	25.7	0.5	69.7
2020	Area [km²]	1.1	2.7	6.6	60.6	1.7	161.3
	Percentage [%]	0.5	1.2	2.7	25.9	0.7	69.0
2021	Area [km²]	1.1	2.7	6.8	58.2	2.2	149.4
	Percentage [%]	0.5	1.2	3.0	26.4	1.0	67.9